eLIFE elifesciences.org

RESEARCH ARTICLE

UBE2G1 governs the destruction of cereblon neomorphic substrates

Gang Lu*, Stephanie Weng†, Mary Matyskiela†, Xinde Zheng, Wei Fang, Scott Wood, Christine Surka, Reina Mizukoshi, Chin-Chun Lu, Derek Mendy, In Sock Jang, Kai Wang, Mathieu Marella, Suzana Couto, Brian Cathers, James Carmichael, Philip Chamberlain, Mark Rolfe

Celgene Corporation, San Diego, United States

Abstract The cereblon modulating agents (CMs) including lenalidomide, pomalidomide and CC-220 repurpose the Cul4-RBX1-DDB1-CRBN ($CRL4^{CRBN}$) E3 ubiquitin ligase complex to induce the degradation of specific neomorphic substrates via polyubiquitination in conjunction with E2 ubiquitin-conjugating enzymes, which have until now remained elusive. Here we show that the ubiquitin-conjugating enzymes UBE2G1 and UBE2D3 cooperatively promote the K48-linked polyubiquitination of $CRL4^{CRBN}$ neomorphic substrates via a sequential ubiquitination mechanism. Blockade of UBE2G1 diminishes the ubiquitination and degradation of neomorphic substrates, and consequent antitumor activities elicited by all tested CMs. For example, UBE2G1 inactivation significantly attenuated the degradation of myeloma survival factors IKZF1 and IKZF3 induced by lenalidomide and pomalidomide, hence conferring drug resistance. UBE2G1-deficient myeloma cells, however, remained sensitive to a more potent IKZF1/3 degrader CC-220. Collectively, it will be of fundamental interest to explore if loss of UBE2G1 activity is linked to clinical resistance to drugs that hijack the $CRL4^{CRBN}$ to eliminate disease-driving proteins.
DOI: https://doi.org/10.7554/eLife.40958.001

***For correspondence:** glu@celgene.com

†These authors contributed equally to this work

Competing interest: See page 21

Funding: See page 21

Received: 10 August 2018
Accepted: 19 September 2018
Published: 20 September 2018

© Copyright Lu et al. This article is distributed under the terms of the Creative Commons Attribution License, which permits unrestricted use and redistribution provided that the original author and source are credited.

Introduction

The ubiquitin-proteasome system (UPS) is a highly regulated component of the protein homeostasis network that dictates multiple cellular processes in eukaryotes (***Hershko and Ciechanover, 1998***). Through the orchestrated actions of ubiquitin-activating enzymes (E1), ubiquitin-conjugating enzymes (E2) and ubiquitin-ligating enzymes (E3), the ε-amine of a lysine residue in a target protein is covalently conjugated with K48- or K11-linked poly-ubiquitin chains, thereby marking the target protein for proteasomal degradation (***Jin et al., 2008***; ***Komander and Rape, 2012***; ***Pickart, 2001***). Recently, repurposing the Cullin-Ring E3 ligase complexes $CRL4^{CRBN}$ (Cul4-RBX1-DDB1-CRBN) and $CRL2^{VHL}$ (Cul2-RBX1-EloB/C-VHL) with small-molecule degraders to remove disease-driving proteins otherwise considered 'undruggable' has emerged as a novel therapeutic modality that has the potential to transform drug discovery and development (***Bondeson and Crews, 2017***; ***Huang and Dixit, 2016***; ***Lebraud and Heightman, 2017***).

There are two types of small-molecule degraders that have been used to date. The first is represented by the immunomodulatory drugs (IMiDs) thalidomide (THAL), lenalidomide (LEN) and pomalidome (POM), as well as other cereblon modulating agents CC-122, CC-220, and CC-885. This class of molecule docks into a tri-tryptophan pocket in the thalidomide-binding domain of cereblon, the substrate receptor of $CRL4^{CRBN}$, to create a hotspot for protein-protein interactions thereby enhancing the binding of unique neomorphic substrate to cereblon, resulting in substrate ubiquitination and degradation (***Fischer et al., 2014***) (***Chamberlain et al., 2014***) (***Matyskiela et al., 2016***) (***Petzold et al., 2016***). All three IMiD drugs promote the degradation of two hematopoietic transcription factors IKZF1 and IKZF3 to achieve anti-myeloma activity (***Krönke et al., 2014***) (***Lu et al.,***

eLife digest Cells routinely breakdown damaged or unwanted proteins to recycle their building blocks. In humans, most of these unwanted proteins are first tagged with a chain of smaller proteins called ubiquitin, in a process known as ubiquitination. Three kinds of enzymes – named E1, E2 and E3 – act one after the other to recruit and transfer ubiquitin onto the protein. Any problem with this protein-disposal system may cause diseases including cancers.

Several drugs such as thalidomide are known to hijack the ubiquitination process by binding to the E3 enzyme. Instead of targeting unwanted proteins, the E3 enzyme-drug complex targets proteins that are driving a disease. These drugs are particularly useful for treating blood cancers. The problem is patients often become resistant to these drugs, and not always because the activity of the E3 enzyme is impaired. An alternative suspect would be an E2 enzyme, but the role of these enzymes remains unclear.

Lu et al. have now asked whether a faulty E2 enzyme can lead to drug resistance in a form of blood cancer called multiple myeloma. The experiments tested how proteins relevant for the growth of cancerous myeloma cells were degraded in the presence of different drugs. Genes for the E2 enzymes were inactivated one at a time using a gene editing approach to see which ones would affect the degradation of the proteins and result in drug resistance. Two E2 enzymes, UBE2G1 and UBE2D3, were found to be critical.

UBE2D3 first links the disease-driving proteins with one ubiquitin before UBE2G1 can subsequently assemble a chain of ubiquitin proteins. If either of these E2 enzymes was missing from myeloma cells treated with drugs, the disease-driving proteins could not be properly tagged with ubiquitin. This interfered with the degradation of the proteins and allowed the myeloma cells to continue to grow. Yet, myeloma cells that did not have UBE2G1 and were resistant to certain drugs could still respond to other more potent drugs. This suggests that the success of the drugs depends on UBE2G1. Therefore, a better understanding of the activity of this E2 enzyme may be useful for the development of future anticancer drugs.

DOI: https://doi.org/10.7554/eLife.40958.002

2014a) (*Gandhi et al., 2014*), whereas only LEN targets CK1α for effective degradation (*Krönke et al., 2015*), which is presumably linked to its efficacy in myelodysplastic syndrome with chromosome 5q deletion. CC-220 is a significantly more potent IKZF1 and IKZF3 degrader than IMiD drugs (*Matyskiela et al., 2018*) (*Nakayama et al., 2017*) (*Schafer et al., 2018*), and it is currently in clinical trials for relapsed/refractory multiple myeloma and systemic lupus erythematosus. By contrast, CC-885 is the only aforementioned cereblon modulating agent that allows cereblon to recognize translation termination factor GSPT1 for ubiquitination and degradation (*Matyskiela et al., 2016*). The second type of small-molecule degraders is generally referred to as a proteolysis-targeting chimera (PROTAC) (*Sakamoto et al., 2001*), which is composed of two linked protein binding ligands, with one engaging a target protein and the other interacting with an E3 ubiquitin ligase such as $CRL4^{CRBN}$ or $CRL2^{VHL}$ to trigger proximity-induced substrate ubiquitination and degradation (*Deshaies, 2015*) (*Neklesa et al., 2017*). Many PROTACs have been described recently, but the clinical value of this approach has not yet been established.

$CRL4^{CRBN}$ belongs to the multi-subunit cullin-RING E3 ubiquitin ligase (CRL) family containing over 200 members (*Petroski and Deshaies, 2005*) (*Lehti et al., 2013*). The mammalian cullin scaffold proteins (including Cul1, Cul2, Cul3, Cul4A, Cul4B, Cul5, and Cul7) bring their substrates into close proximity with E2 ubiquitin-conjugating enzymes, thereby enabling effective substrate ubiquitination (*Petroski and Deshaies, 2005*) (*Lehti et al., 2013*). $SCF(Skp1\text{-}Cul1\text{-}F\text{-}box)^{Cdc4}$, the founding member of the cullin-RING E3 ligase family, was first discovered in the budding yeast *Saccharomyces cerevisiae*, in which SCF^{Cdc4} works in conjunction with a single E2 ubiquitin-conjugating enzyme Cdc34 to promote the polyubiquitination of a variety of SCF substrates (*Feldman et al., 1997*) (*Skowyra et al., 1997*) (*Blondel et al., 2000*) (*Jang et al., 2001*; *Perkins et al., 2001*). Human Cdc34/UBE2R1 can substitute for yeast Cdc34 in *Saccharomyces cerevisiae* underscoring their functional conservation (*Plon et al., 1993*). However, in contrast to its dominant role in catalyzing the ubiquitination of SCF substrates in yeast, Cdc34 coordinates ubiquitination with UBE2D3/UbcH5c

via a sequential ubiquitination mechanism to improve reaction rate and efficiency in human cells. In brief, Cdc34 acts as an ubiquitin chain elongation enzyme that assembles the K48-linked ubiquitin chains on mono-ubiquitins pre-conjugated to SCF substrates by UBE2D3 (**Pan et al., 2004**). Such sequential ubiquitination by two E2 enzymes was first reported for the anaphase-promoting complex ubiquitin ligase (**Rodrigo-Brenni and Morgan, 2007**). More recently, the RING1-IBR-RING2 (RBR) E3 ligase ARIH1 was shown to tag client substrates of CRL1, CRL2 and CRL3 with monoubiquitin, thereby enabling CDC34-dependent K48-linked ubiquitin chain elongation (**Scott et al., 2016**). This finding points to a potentially more prevailing mechanism of ubiquitin chain priming and extending carried out by two distinct E2s. Several ubiquitin conjugation E2 enzymes have been reported to regulate CRL4 substrates as well. For instance, in response to UV irradiation, the $CRL4^{Cdt2}$ ligase complex mediates the proteolysis of Cdt1 with the help of E2 enzymes UBE2G1 and its paralog UBE2G2, while working together with a different E2 enzyme UbcH8/UBEL6 to trigger the degradation of p21 and Set8 in human cells (**Shibata et al., 2011**). Despite the proven cellular efficacy and clinical success of many cereblon modulating agents, it remain unknown whether unique ubiquitin E2 enzymes control the ubiquitination of each specific cereblon neomorphic substrate, and whether loss of E2 enzymes contributes to resistance to these agents.

Results

UBE2G1 is the dominant ubiquitin E2 enzyme that governs the destruction of cereblon neomorphic substrates induced by cereblon modulating agents

The clinical course of multiple myeloma typically follows a recurring pattern of remission and relapse with resistance to IMiD drugs based combination regimens (**Harousseau and Attal, 2017**). Such relapse is not frequently associated with cereblon downregulation and/or mutation (**Kortüm et al., 2016**; **Qian et al., 2018**) (**Zhu et al., 2011**). Hence, we reasoned that resistance to IMiD drugs in myeloma could be ascribed to reduced degradation of IKZF1 and IKZF3 as a result of inactivation of other essential components of the $CRL4^{CRBN}$ ligase complex, for instance the E2 ubiquitin conjugation enzyme. To look for such proteins, we devised a high-throughput CRISPR-Cas9 screen approach to monitor the effect of individual knockout of a gene of interest on POM-induced degradation of IKZF1 protein tagged with enhanced ProLabel (ePL), a small β-galactosidase N-terminal fragment (**Figure 1A**), and created a single guide RNA (sgRNA) library containing three sgRNAs for each of the 41 annotated E2 enzymes in the human genome, as well as three non-targeting sgRNAs in arrayed format (**Supplementary file 1**). The ePL tag complements with the large β-galactosidase C-terminal fragment to form an active enzyme that hydrolyzes substrate to emit a chemiluminescent signal, allowing the measurement of ePL-IKZF1 fusion protein level in a high-throughput fashion.

To determine the robustness of this screening approach, we transduced U937 cells stably expressing Cas9 and ePL-IKZF1 (U937_Cas9_ePL-IKZF1) with lentiviral vector expressing a non-targeting or *CRBN*-specific sgRNA. We chose U937 cells for assessing the effect of individual gene knockout on POM-induced IKZF1 degradation because we were able to express the ePL-tagged IKZF1 fusion protein below the level of endogenous IKZF1 protein and POM can induce the efficient degradation of both endogenous and ePL-tagged IKZF1 (**Figure 1—figure supplement 1**). Four days post transduction, cells were seeded into 384-well plates pre-dispensed with either DMSO vehicle control or POM at varying concentrations. Sixteen hours after incubation, IKZF1 degradation was assessed using the ePL luminescent assay. As expected, cereblon knockout completely abrogated the degradation of ePL-tagged IKZF1 fusion protein (**Figure 1—figure supplement 1**). Using this approach we then evaluated the effect of individual knockout of each E2 enzyme on ePL-IKZF1 degradation induced by POM. Out of 41 E2 enzymes, UBE2G1 and to a lesser extent UBE2M, UBE2D3, and UBE2D2/UbcH5b, when depleted, imposed statistically significant inhibition on the ePL-IKZF1 degradation (**Figure 1B**, and **Figure 1—figure supplement 2D,F,I**).

UBE2M, also called UBC12, is a NEDD8-conjuating enzyme, which regulates, via neddylation, the activity of all Cullin Ring E3 ligases including $CRL4^{CRBN}$ (**Petroski and Deshaies, 2005**) (**Gong and Yeh, 1999**) (**Pan et al., 2004**). Indeed, MLN4924, an inhibitor of NEDD8-activating enzyme (**Soucy et al., 2009**), prevented the degradation of ePL-IKZF1 induced by POM (**Figure 1—figure supplement 2V**). The effect of UBE2M knockout, however, was much less pronounced (**Figure 1—**

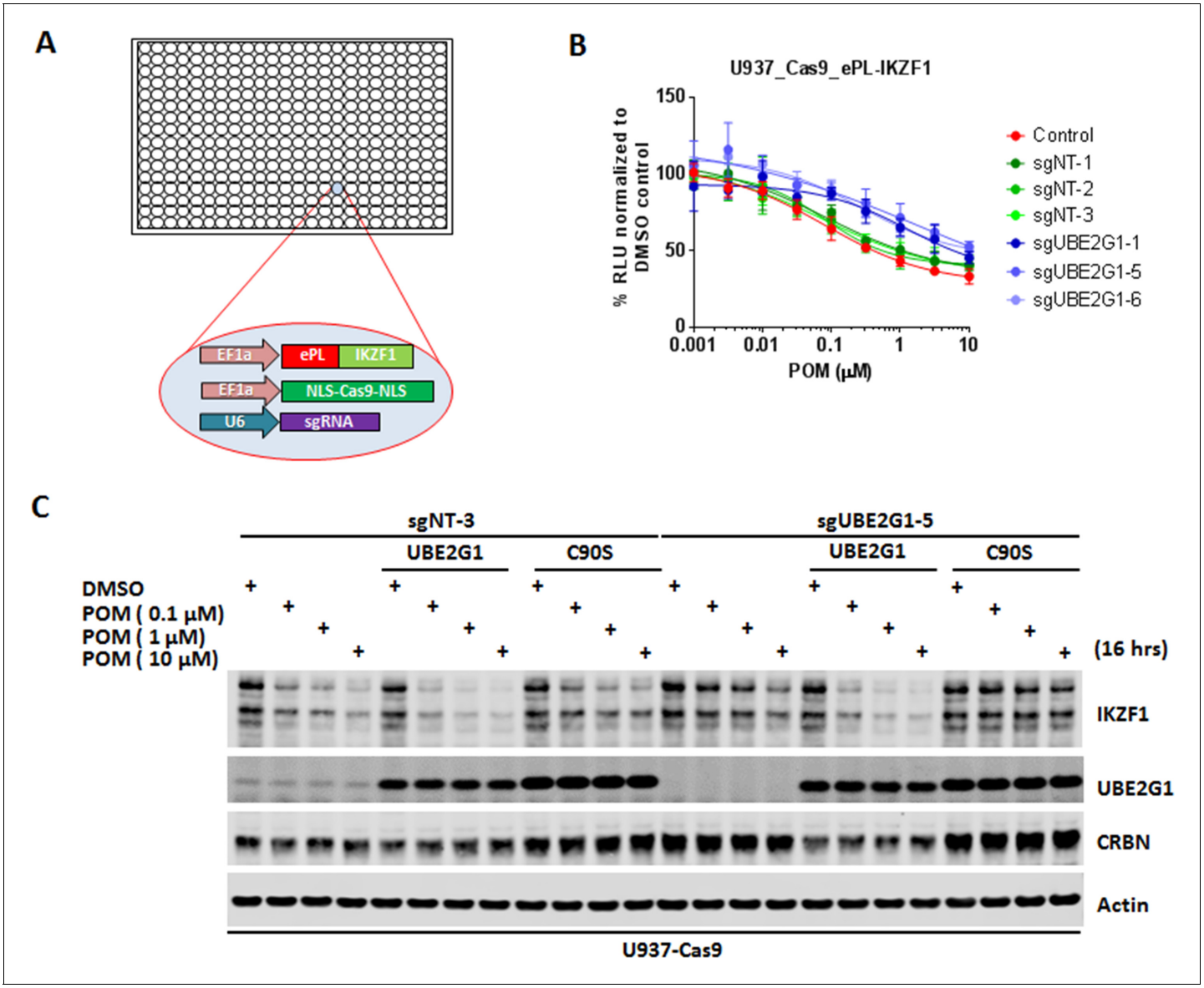

Figure 1. Identification of UBE2G1 as the most critical ubiquitin E2 enzyme that mediates the pomalidomide-induced degradation of IKZF1. (**A**) Schematic showing the design of the CRISPR screen to identify E2 enzyme(s) regulating the CM-induced degradation of ePL-tagged IKZF1 in 384-well array format. (**B**) Chemiluminescent measurement of ePL-IKZF1 protein expression level in U937_Cas9_ePL-IKZF1 parental cells or cells expressing non-targeting or *UBE2G1*-specific sgRNAs. Cells were treated with POM at the indicated concentrations for 16 hr. Data are presented as mean ± SD, n = 4 technical replicates. (**C**) Immunoblot analysis of U937_Cas9 parental or *UBE2G1-/-* cells with or without stable expression of UBE2G1 wild-type or C90S mutant. Cells were treated with POM at the indicated concentrations for 16 hr. Result is representative of three independent experiments.

DOI: https://doi.org/10.7554/eLife.40958.003

The following source data and figure supplements are available for figure 1:

Source data 1. ePL luminescence signal shown in ***Figure 1B***.

DOI: https://doi.org/10.7554/eLife.40958.008

Figure supplement 1. Pomalidomide-induced destruction of IKZF1 requires $CRL4^{CRBN}$.

DOI: https://doi.org/10.7554/eLife.40958.004

Figure supplement 1—source data 1. ePL luminescence signal shown in ***Figure 1—figure supplement 1A***.

DOI: https://doi.org/10.7554/eLife.40958.005

Figure supplement 2. The effect of individual knockout of each of the 41 annotated E2 enzymes or inactivation of cullin neddylation with MLN4924 on pomalidomide-induced destruction of IKZF1.

DOI: https://doi.org/10.7554/eLife.40958.006

Figure 1 continued on next page

Figure 1 continued

Figure supplement 2—source data 1. ePL luminescence signal shown in ***Figure 1—figure supplement 2A–V***, and CTG luminescence signal shown in ***Figure 1—figure supplement 2W***.

DOI: https://doi.org/10.7554/eLife.40958.007

figure supplement 2I). Given the well-established role of UBE2M in cell proliferation and survival, we reasoned that this difference could be explained by that U937 cells only with partial UBE2M loss survived four days after CRISPR gene editing. Consistent with this notion, cellular fitness was markedly reduced by 48 hr treatment of MLN2924 at concentrations that elicited near-complete blockage of POM-induced IKZF1 degradation in the U937_Cas9_ePL-IKZF1 cell line used in the screen (***Figure 1—figure supplement 2V,W***).

CRISPR knockout of UBE2G1 also attenuated the destabilization of endogenous IKZF1 by POM in U937 cells, and this defect could be rescued by wild-type UBE2G1, but not a UBE2G1 enzymatically-dead mutant (C90S, ***Figure 1C***). Knockout of UBE2D3, on the other hand, showed very little effect on the degradation of endogenous IKZF1 (***Figure 2C***). Thus, we reasoned that there are additional E2 enzyme(s) modulating the degradation of IKZF1 cooperatively with UBE2G1. To identify such E2 (s), we evaluated the effect of double knockout of UBE2G1 and one of the 41 E2 enzymes on IKZF1 degradation using a dual gRNA-directed gene knockout approach (***Figure 2A*** and ***Figure 2—figure supplement 1***). Notably, double knockout of UBE2G1 and UBE2D3 produced more inhibition of POM-induced degradation of ePL-tagged and endogenous IKZF1 than either single knockout alone (***Figure 2B and C***). Combinatorial ablation of UBE2G1 with UBE2E1 or UBE2M also demonstrated subtle but noticeable further inhibition on IKZF1 degradation (***Figure 2—figure supplement 1E,I***). Although UBE2D2 knockout slightly attenuated the POM-induced ePL-IKZF1 degradation (***Figure 1—figure supplement 2D***), double knockout of UBE2D2 and UBE2G1 did not significantly augment the inhibition of ePL-IKZF1 degradation imposed by UBE2G1 single knockout (***Figure 2—figure supplement 1D***).

To assess the substrate selectivity of UBE2G1, we determined the effect of UBE2G1 knockout on the degradation of IKZF1, its paralog IKZF3 and other well-characterized cereblon neomorphic substrates, triggered by their respective cereblon modulating agents including cereblon-based PROTACs. Ablation of UBE2G1 significantly diminished the degradation of IKFZ1 (***Figure 3A***, and ***Figure 3—figure supplement 1A,B***), IKZF3 (***Figure 3A***, and ***Figure 3—figure supplement 1A,B***) and ZFP91 (Figure 7B, and Figure 7—figure supplement 1B,D) by LEN, POM, and CC-220, as well as CK1α degradation (Figure 7B, and Figure 7—figure supplement 1B,D) by LEN in OPM2, DF15 and MM1S myeloma cells. UBE2G1 loss also reduced the degradation of GSPT1 induced by CC-885 in myeloma cell lines OPM2, DF15 and MM1S (***Figure 3B***, and ***Figure 3—figure supplement 1C,D***), AML cell lines OCI-AML2, U937, MOLM-13 and MV4-11 (***Figure 3—figure supplement 1E–H***), as well as 293T human embryonic kidney cells (***Figure 3—figure supplement 1I***). The GSPT1 degradation defect conferred by UBE2G1 depletion could also be rescued by UBE2G1 wild-type but not C90S mutant in 293 T cells (***Figure 3—figure supplement 1I***). UBE2G1 loss also blocked the degradation of BRD4 induced by the cereblon-based BET PROTAC dBET1 (***Winter et al., 2015***), but not the VHL-based BET PROTAC MZ1 (***Zengerle et al., 2015***) in 293 T cells (***Figure 3C***). Consistently, UBE2G1 depletion prolonged the protein half-lives of IKZF1 and IKZF3 in OPM2 cells treated with POM (***Figure 3D***). Lastly, UBE2G1 loss did not affect stability of SCF substrates p27 and c-Myc, indicating the specific regulation of $CRL4^{CRBN}$ by UBE2G1 (***Figure 3D***).

UBE2G1 mediates the ubiquitination of cereblon neomorphic substrates

UBE2G1 and its paralog UBE2G2 share similar domain structures with CDC34. A common structural feature of these three E2 enzymes is an acidic loop (***Figure 4—figure supplement 1A***, highlighted with red) in the vicinity of their respective active site cysteines (***Figure 4—figure supplement 1A***, highlighted with blue), which facilitates the direct binding with ubiquitin and enables K48-linked ubiquitin chain assembly in the absence of associated E3 ligases (***Choi et al., 2015***). In association with gp78, an ER membrane bound RING finger E3 ubiquitin ligase, UBE2G2 directly tags misfolded proteins with K48-linked ubiquitin chains preassembled on the catalytic cysteine of UBE2G2,

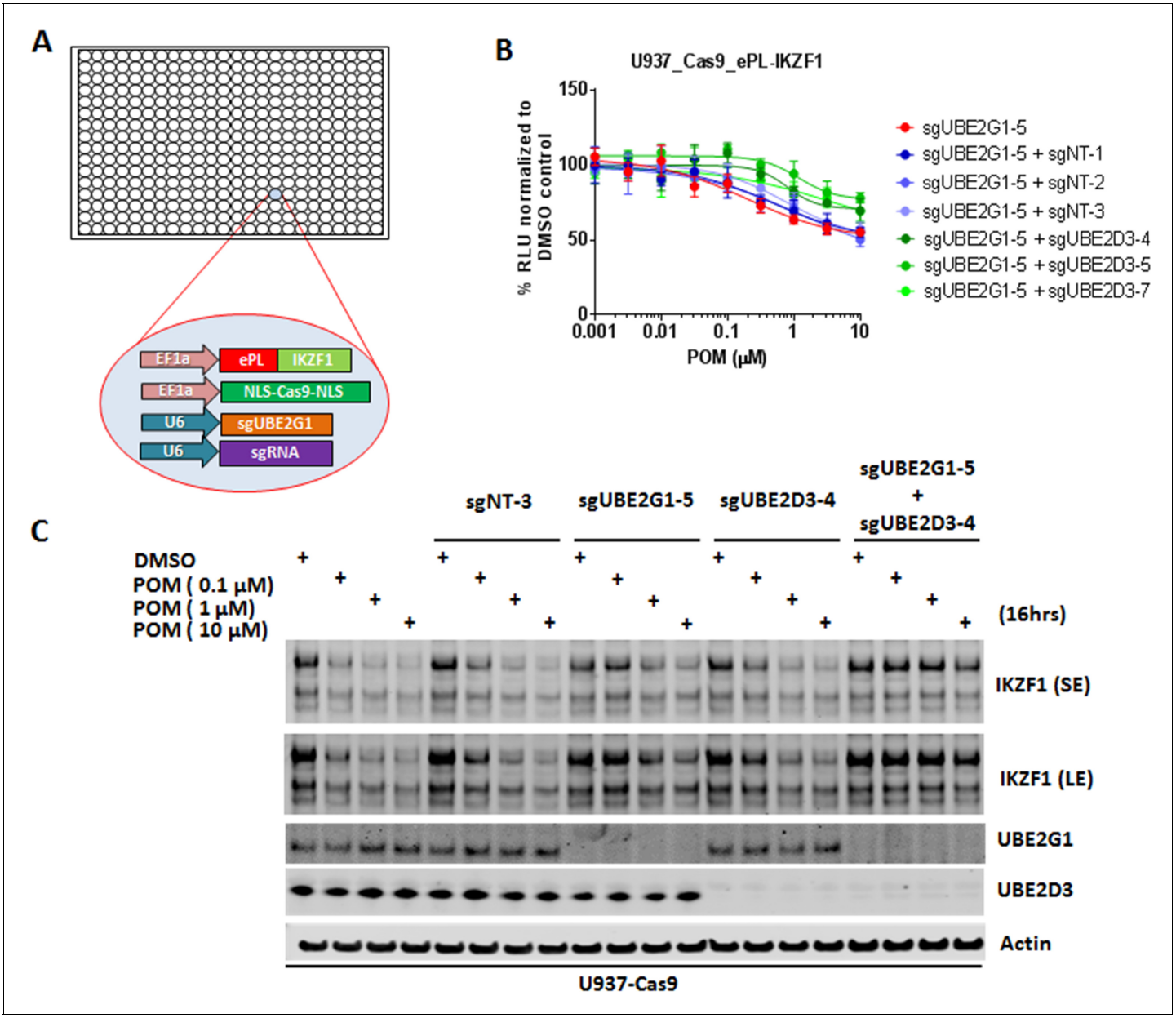

Figure 2. UBE2G1 and UBE2D3 redundantly regulate the pomalidomide-induced degradation of IKZF1. (**A**) Schematic showing the design of dual-gRNA directed CRISPR screen of E2s regulating the CM-induced degradation of ePL-tagged IKZF1 in 384-well array format. (**B**) Chemiluminescent measurement of ePL-IKZF1 protein expression level in U937_Cas9_ePL-IKZF1 parental cells or cells expressing *UBE2G1*-specfic sgRNA alone or in combination with non-targeting or *UBE2D3*-specific sgRNA. Cells were treated with POM at the indicated concentrations for 16 hr. Data are presented as mean ± SD, n = 4 technical replicates. (**C**) Immunoblot analysis of U937-Cas9 parental cells or cells expressing non-targeting sgRNA, *UBE2G1*-specific sgRNA, *UBE2D3*-specfic sgRNA, or both *UBE2G1* and *UBE2D3* sgRNAs. Cells were treated with POM at the indicated concentrations for 16 hr. SE, short exposure; LE, long exposure. Result is representative of three independent experiments.

DOI: https://doi.org/10.7554/eLife.40958.009

The following source data and figure supplements are available for figure 2:

Source data 1. ePL luminescence signal shown in ***Figure 2B***.

DOI: https://doi.org/10.7554/eLife.40958.012

Figure supplement 1. The effect of double knockout of UBE2G1 and one of the 41 E2 enzymes on pomalidomide-induced destruction of IKZF1.

DOI: https://doi.org/10.7554/eLife.40958.010

Figure supplement 1—source data 1. ePL luminescence signal shown in ***Figure 2—figure supplement 1A–U***.

DOI: https://doi.org/10.7554/eLife.40958.011

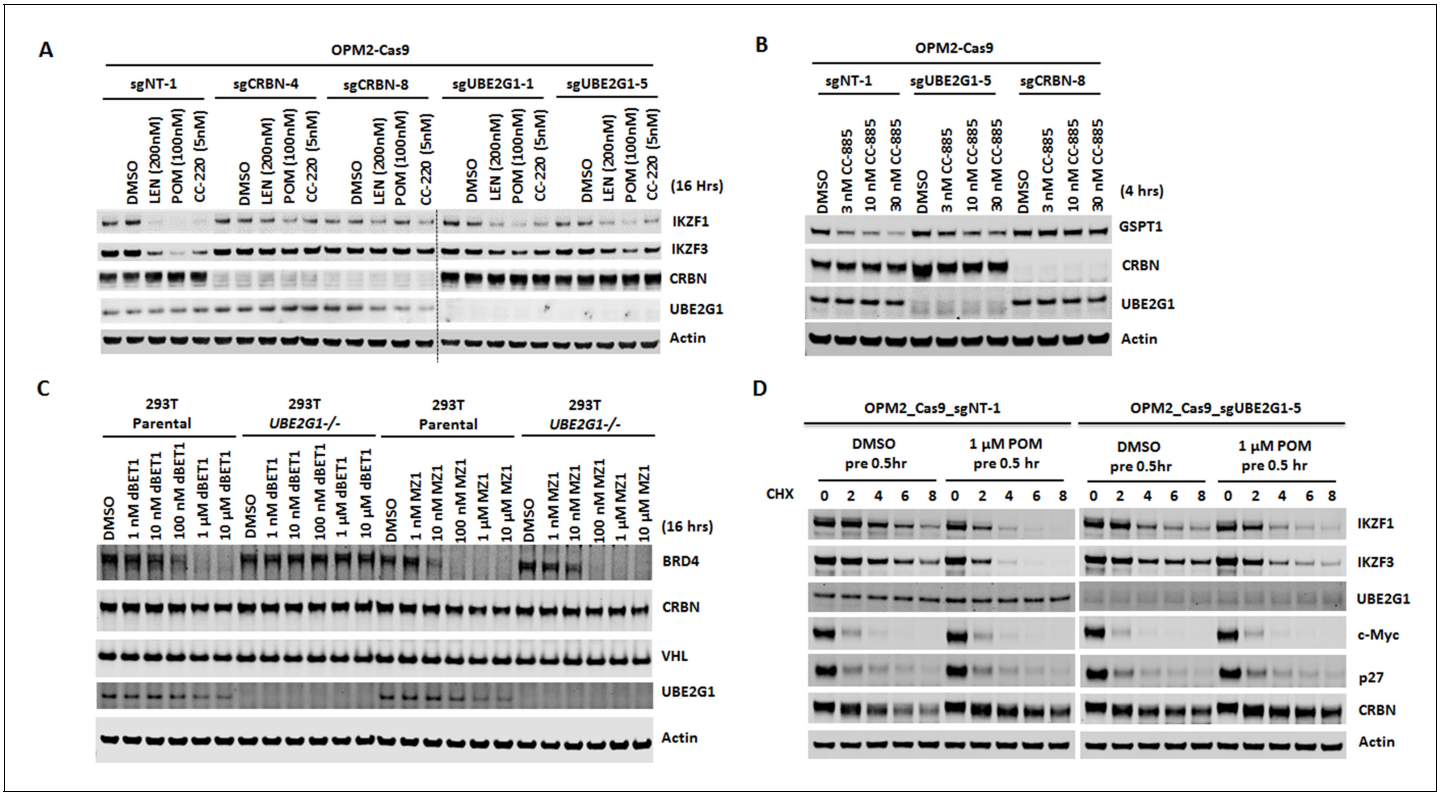

Figure 3. Loss of UBE2G1 blocked the degradation of cereblon neomorphic substrates induced by cereblon-modulating agents. (**A and B**) Immunoblot analysis of OPM2-Cas9 cells expressing non-targeting, *UBE2G1*-specific or *CRBN*-specific sgRNA. Cells were treated with LEN, POM or CC-220 for 16 hr (**A**) or CC-885 for 4 hr (**B**) at the indicated concentrations. (**C**) Immunoblot analysis of 293T parental or *UBE2G1-/-* cells treated with BRD4 PROTACs dBET1 or MZ1 at the indicated concentrations for 16 hr. (**D**) Immunoblot analysis of OPM2 parental or *UBE2G1-/-* cells treated with 100 μg/ml cycloheximide with or without 1 μM POM pretreatment for half an hour. Cells were harvested at the indicated time points. All results shown in this figure are representative of three independent experiments.

DOI: https://doi.org/10.7554/eLife.40958.013

The following figure supplements are available for figure 3:

Figure supplement 1. Elimination of UBE2G1 blocks the degradation of cereblon neomorphic substrates recruited by lenalidomide and CC-885.

DOI: https://doi.org/10.7554/eLife.40958.014

Figure supplement 2. Depletion of UBE2G1 attenuated the degradation of p21 and RMB39 induced by UV irradiation and sulfonamide treatment, respectively.

DOI: https://doi.org/10.7554/eLife.40958.015

resulting in ER associated protein degradation (ERAD) (***Li et al., 2007***). Although it has been shown that UBE2G1 and UBE2G2 redundantly mediate the destabilization of the $CRL4^{Cdt2}$ substrate Cdt1 in response to UV irradiation, the direct transfer of ubiquitin to Cdt1 by UBE2G1 or UBE2G2 has not been demonstrated (***Shibata et al., 2011***).

Next, we employed a reconstituted in vitro ubiquitination assay to address the role of UBE2G1 and UBE2D3 in ubiquitination of IKZF1 and GSPT1 induced by POM and CC-885, respectively. We monitored the production of ubiquitin conjugates of IKZF1 and GSPT1 catalyzed by UBE2D3 alone, UBE2G1 alone, or in combination, in the presence of Ube1 (E1), Cul4-Rbx1, cereblon-DDB1, ubiquitin and ATP with or without POM or CC-885. UBE2D3 alone produced ubiquitin conjugates of IKZF1 or GSPT1 mainly with a single or di-ubiquitin moiety in a POM-or CC-885- dependent manner (***Figure 4A and B***, lanes 1 and 2). By contrast, UBE2G1 alone failed to display any ubiquitin conjugating activity for both IKZF1 and GSPT1 (***Figure 4A and B***, lanes 3 and 4). However, when combined with UBE2D3, UBE2G1 significantly promoted the extent of ubiquitination of both substrates (***Figure 4A and B***, lanes 2 and 6). Moreover, the ubiquitin conjugates of IKZF1 or GSPT1 formed with both UBE2G1 and UBE2D3, but not UBE2D3 alone, were exclusively K48-linked, because the wild-type ubiquitin used in the reconstituted ubiquitination reaction could be functionally replaced

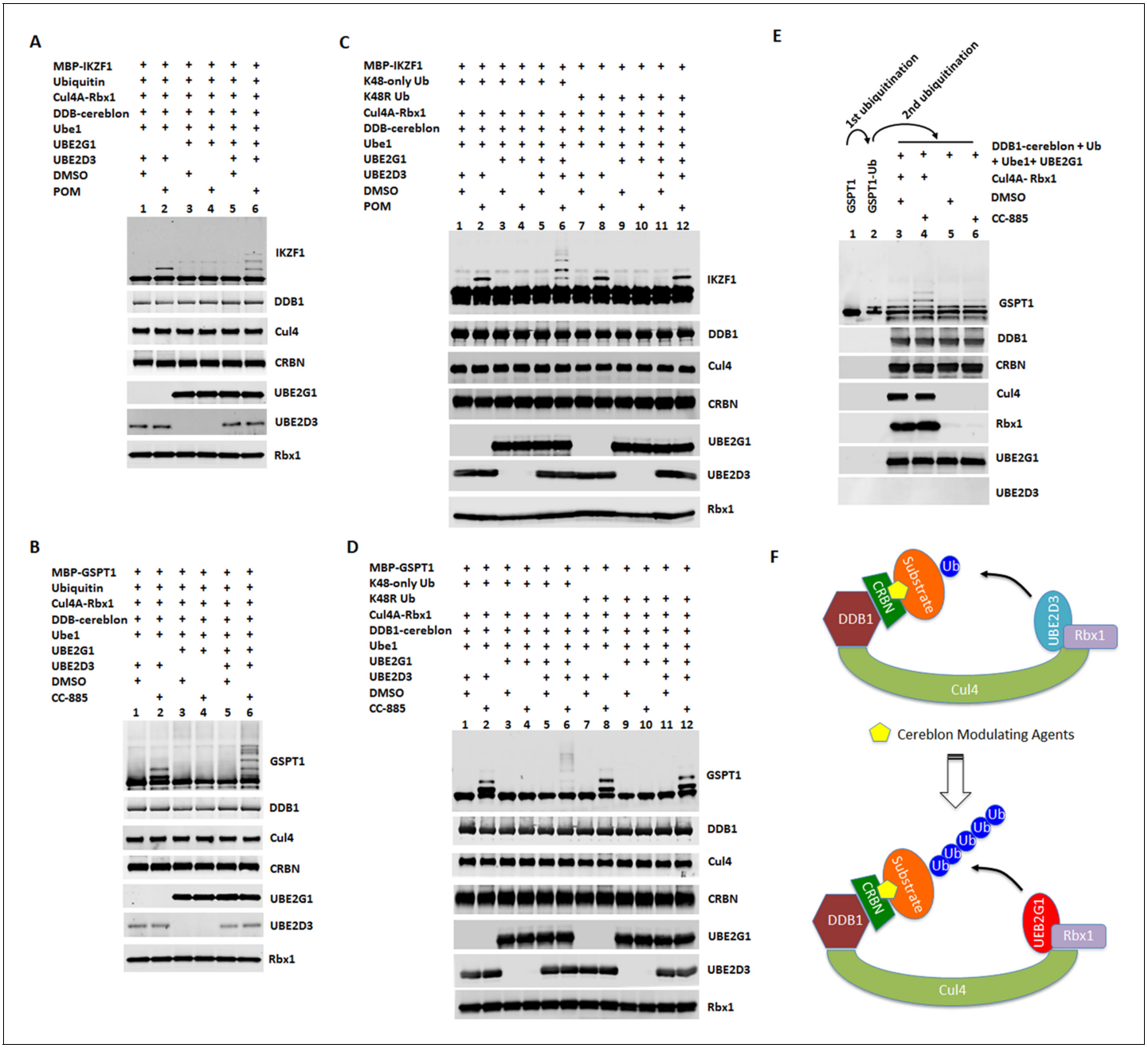

Figure 4. UBE2G1 and UBE2D3 sequentially catalyze the in vitro ubiquitination of IKZF1 and GSPT1 in the presence of pomalidomide and CC-885, respectively. (**A– D**) In vitro ubiquitination of IKZF1 (**A and C**) and GSPT1 (**B and D**) MBP fusion proteins by recombinant $CRL4^{CRBN}$ complex. Recombinant protein products as indicated were incubated with or without 80 μM POM (**A and C**) or 80 μM CC-885 (**B and D**) in the ubiquitination assay buffer containing 80 mM ATP at 30˚C for 2 hr, and then analyzed by immunoblotting. (**E**) Sequential in vitro ubiquitination of GSPT1 by recombinant $CRL4^{CRBN}$ complex. MBP-GSPT1 recombination protein was incubated with Ube1, UBE2D3, Cul4-Rbx1, DDB1-cereblon, Ubiquitin, ATP and CC-885 in the ubiquitination assay at 30˚C for 4 hr. After purification over size-exclusion chromatography, pre-ubiquitinated MBP-GSPT1 protein was then incubated with Ube1, DDB1-cereblon, Ubiquitin, ATP and UBE2G1 with or without CC-885 or Cul4A-Rbx1 in the ubiquitination assay at 30˚C for 2 hr, followed by immunoblot analysis. (**F**) Schematic showing the sequential ubiquitination of CRBN neomorphic substrates by UBE2D3 and UBE2G1. Results shown in (**A–E**) are representative of three independent experiments.

DOI: https://doi.org/10.7554/eLife.40958.016

The following figure supplements are available for figure 4:

Figure supplement 1. UBE2G1 catalyzes the ubiquitin chain assembly on GSPT1 pre-conjugated with ubiquitin.

DOI: https://doi.org/10.7554/eLife.40958.017

Figure supplement 2. UBE2D family proteins redundantly promote the ubiquitination of GSPT1.

Figure 4 continued on next page

Figure 4 continued

DOI: https://doi.org/10.7554/eLife.40958.018

by ubiquitin mutant K48-only (with six remaining lysine residues mutated to arginine) (***Figure 4C and D***, lanes 2 and 6), but not by K48R (remaining lysine residues were intact) (***Figure 4C and D***, lanes 8 and 12), and the ubiquitination pattern of IKZF1 or GSPT1 catalyzed by UBE2D3 exhibited no obvious difference between wild-type ubiquitin and K48-only or K48R mutant (***Figure 4A and B***, lane 2; ***Figure 4C and D***, lanes 2 and 8).

To further explore the mechanism underlying the cooperativity between UBE2G1 and UBE2D3, we separated the ubiquitination reaction of GSPT1 into two steps. First, following GSPT1 ubiquitination by UBE2D3 alone, we isolated GSPT1 ubiquitin conjugates from the rest of reaction components using a size-exclusion column (***Figure 4E***, lanes 1 and 2). We then incubated the purified GSPT1 ubiquitin conjugates with UBE2G1, Ube1 (E1), cereblon-DDB1, ubiquitin and ATP with or without CC-885 and Cul4-Rbx1. We found that UBE2G1 was capable of catalyzing the further ubiquitination of GSPT1 only with prior-conjugated ubiquitin (***Figure 4E***, lanes 1–4, note the conversion of the mono-ubiquitinated GSPT1 into di- or tri-ubiquitinated forms), and this action required the presence of CC-885 and Cul4A-Rbx1 (***Figure 4E***, lanes 3–6).

To rule out the possibility that the UBE2G1 function observed above is simply an artifact of bacterial recombinant protein, we reconstituted the ubiquitination reaction using FLAG-tagged UBE2G1 and FLAG-tagged UBE2D3 proteins purified from 293T *UBE2G1-/-* cells, in which ectopic overexpression of FLAG-tagged UBE2G1 and UBE2D3, but not their respective enzymatically-dead mutant, could partially rescue the defect in CC-885-induced GSPT1 degradation elicited by UBE2G1 loss (***Figure 4—figure supplement 1B***). In agreement with our previous findings, GSPT1 ubiquitination catalyzed in vitro by FLAG-UBE2G1 and FLAG-UBE2D3, alone or in combination, was similar to what was observed with bacterial recombinant UBE2G1 and UBE2D3 (***Figure 4—figure supplement 1C***). In addition, we examined the in vivo function of UBE2G1 and UBE2D3 in the regulation of POM-induced ubiquitination of IKZF1 ectopically expressed in 293 T cells. Ablation of both UBE2G1 and UBE2D3 significantly reduced, but did not completely block, the mono- and polyubiquitination of IKZF1 induced by POM, indicating the existence of additional E2 enzymes with redundant function (***Figure 5A*** and ***Figure 5—figure supplement 1A***). Reintroduction of UBE2G1 alone via transient transfection in 293T *UBE2G1-/-; UBE2D3-/-* cells dramatically enhanced the extent of POM-induced IKZF1 polyubiquitination (***Figure 5B*** and ***Figure 5—figure supplement 1B***, lanes 5–8 vs 1–4). Transient overexpression of UBE2D3 alone promoted IKZF1 monoubiquitination as well as polyubiquitination but to a lesser extent (***Figure 5B*** and ***Figure 5—figure supplement 1B***, lanes 9–12 vs 1–4). Overexpression of both achieved an additive or possibly synergistic effect on IKZF1 ubiquitination (***Figure 5B*** and ***Figure 5—figure supplement 1B***, lanes 13–16 vs 5–12, note the conversion of monoubiquinated IKZF1 into its polyubiquitinated forms). In keeping with the in vitro finding (***Figure 4A***), IKZF1 was mainly mono-ubiquitinated in 293T *UBE2G1-/-* cells following POM treatment, and UBE2G1 wild-type but not C90S mutant could restore IKZF1 polyubiquitination (***Figure 5C*** and ***Figure 5—figure supplement 1C***).

UBE2G1 loss confers resistance to cereblon modulating agents

Since UBE2G1 depletion significantly attenuated the degradation of all cereblon neomorphic substrates, we reasoned that UBE2G1 protein downregulation, gene deletion or mutation might lead to reduced $CRL4^{CRBN}$ activity, thereby leading to resistance to cereblon modulating agents. To test this hypothesis, we surveyed the protein expression level of UBE2G1 in myeloma cell lines with variable sensitivity to LEN and POM (***Figure 6A***). LEN sensitive cell lines MM1S, OPM2, DF15 and NCI-H929 displayed higher expression level of UBE2G1 than LEN medium-sensitive cell line ANABL-6 and LEN resistant cell lines EJM, L363, SKMM-2, CAG and ARH-77, and more strikingly UBE2G1 expression in SKMM-2 was undetectable (***Figure 6B***). As expected, reintroduction of UBE2G1 wild-type but not C90S mutant significantly augmented the antiproliferative effect of both LEN and POM, which was linked to the enhanced degradation of IKZF1 and IKZF3 (***Figure 6C and D***). UBE2G1 loss also conferred resistance to CC-885 in OCI-AML2, U937, MOLM-13, and MV4-11 AML cells (***Figure 6—figure supplement 1A–D***), as well as 293 T cells, and this defect could be rescued by UBE2G1 wild-

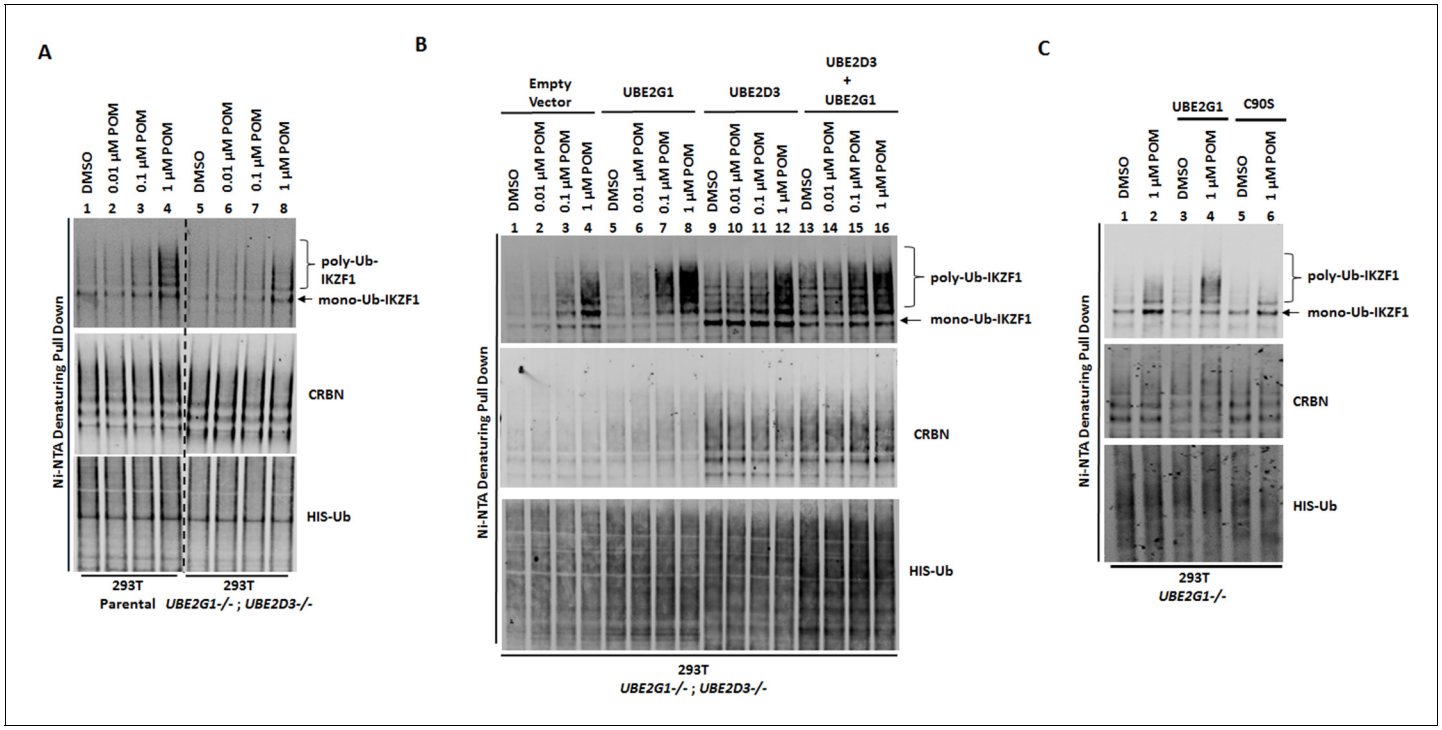

Figure 5. UBE2G1 and UBE2D3 cooperatively promote the in vivo ubiquitination of IKZF1. (**A and B**) 293T parental and *UBE2G1-/-;UBE2D3-/-* (clone 4) cells were transiently transfected with plasmids expressing cereblon, V5-tagged IKZF1 and 8xHis-Ub with or without UBE2G1, UBE2D3 or both. (**C**) 293T parental and *UBE2G1-/-* (clone 13) cells were transiently transfected with plasmids expressing cereblon, IKZF1-V5, 8xHis-Ub with or without UBE2G1 wild-type or C90S mutant. In (**A**), (**B**) and (**C**), 48 hr after transfection, cells were treated with MG-132 (10 µM) and POM at the indicated concentrations for additional 8 hr. Ubiquitinated protein products enriched with magnetic nickel sepharose were subjected to immunoblot analysis. Immunoblot analysis of whole cell extracts showing equal input proteins is shown in ***Figure 5—figure supplement 1A-C***. All results shown in this figure are representative of three independent experiments.

DOI: https://doi.org/10.7554/eLife.40958.019

The following figure supplement is available for figure 5:

Figure supplement 1. Input protein levels for the in vivo ubiquitination studies corresponding to ***Figure 5***.

DOI: https://doi.org/10.7554/eLife.40958.020

type but not C90S mutant (***Figure 6—figure supplement 1E***). Moreover, UBE2G1 deletion conferred resistance to BET PROTAC dBET1 but not MZ1 in 293 T cells (***Figure 6—figure supplement 1F***). Lastly, UBE2G1 knockout in DF15, MM1S and OPM2 myeloma cells conferred significant resistance to LEN and POM (***Figure 7A***, and ***Figure 7—figure supplement 1A,C***-). Importantly, these cells were only partially resistant to CC-220, in keeping with the increased efficiency in triggering IKZF1 and IKZF3 degradation (***Figure 7A and B*** and ***Figure 7—figure supplement 1A–D***). These results indicate that UBE2G1 deficiency may be a key differentiator in the clinical success of cereblon modulating agents.

Discussion

The sequential recruitment of two functionally distinct E2s by a single E3 is a general mechanism for substrate ubiquitination conserved from yeast to human (***Rodrigo-Brenni and Morgan, 2007***) (***Wu et al., 2010***) (***Kleiger and Deshaies, 2016***). In this work, we provide evidence that $CRL4^{CRBN}$ deploys the same mechanism to mark its neomorphic substrates with K48-linked poly-ubiquitin chains for proteasomal degradation. Mechanistically, UBE2D3 transfers the first ubiquitin onto the lysine residue(s) of the cereblon neomophic substrate, thereby enabling UBE2G1 to assemble the K48-linked ubiquitin chains onto the initial anchor ubiquitin (***Figure 4F***). This orchestrated action between UBE2D3 and UBE2G1 closely resembles the cooperativity of UBE2D3 and Cdc34 in promoting IκBα polyubiquitination mediated by $SCF^{\beta TRCP2}$ (***Wu et al., 2010***), except that unlike Cdc34,

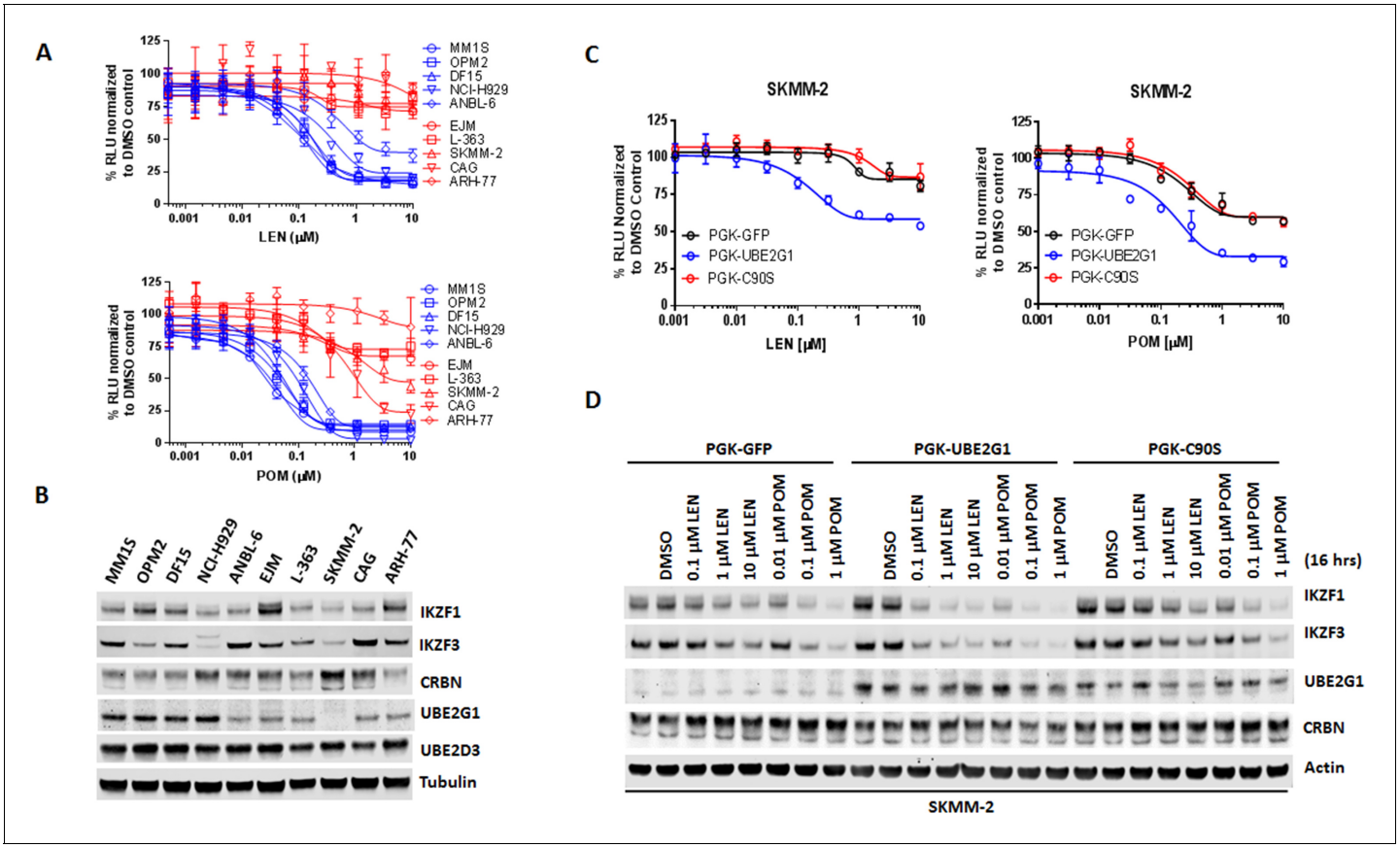

Figure 6. UBE2G1 loss confers resistance to lenalidomide and pomalidomide in myeloma cell lines. (**A**) Effect of LEN (top panel) and POM (bottom panel) on proliferation of myeloma cell lines. Cell proliferation was determined by CTG. Data are presented as mean ± SD, n = 3 technical replicates. (**B**) Immunoblot analysis of myeloma cell lines used in (**A**). (**C and D**) Proliferation (**C**) and immunoblot analysis (**D**) of SKMM2 cells transduced with lentiviral vectors encoding GFP, UBE2G1 and UBE2G1-C90S. Cells were treated with DMSO vehicle control, LEN or POM at the indicated concentrations for 5 days (**C**) or 16 hr (**D**). In (**C**), cell proliferation was determined by CTG, and data are presented as mean ± SD, n = 3 technical replicates. All results shown in this figure are representative of three independent experiments.

DOI: https://doi.org/10.7554/eLife.40958.021

The following source data and figure supplements are available for figure 6:

Source data 1. CTG luminescence signal shown in ***Figure 6A,C***.

DOI: https://doi.org/10.7554/eLife.40958.024

Figure supplement 1. The growth-inhibitory effect of CC-885 and BRD4 PROTACs in AML cell lines and 293 T cells.

DOI: https://doi.org/10.7554/eLife.40958.022

Figure supplement 1—source data 1. CTG luminescence signal shown in ***Figure 6—figure supplement 1A–F***.

DOI: https://doi.org/10.7554/eLife.40958.023

UBE2G1 does not possess the ability to transfer ubiquitin onto substrates without prior ubiquitin conjugation. UBE2G1 was known to produce K48-linked poly-ubiquitin chains in the absence of an E3 ubiquitin ligase (***Choi et al., 2015***), but UBE2G1 cannot promote GSPT1 ubiquitination in the absence of CC-885 or Cul4A-Rbx1 (***Figure 4E***), indicating that close proximity of UBE2G1 to cereblon neomorphic substrates bridged by $CRL4^{CRBN}$ is required to increase the processivity of UBE2G1 at physiological concentrations. This provides an explanation to how cereblon modulating agents can induce effective substrate degradation via K48-linked polyubiquitination, as well as speaks to the potential role of UBE2G1 in mediating the ubiquitination and degradation of other CRL4 cognate and/or neomorphic substrates. This is supported by the impaired degradation of p21 and RBM39 induced by UV irradiation and E7070 treatment, respectively, in 293T *UBE2G1-/-* cells (***Figure 3—figure supplement 2A,B***).

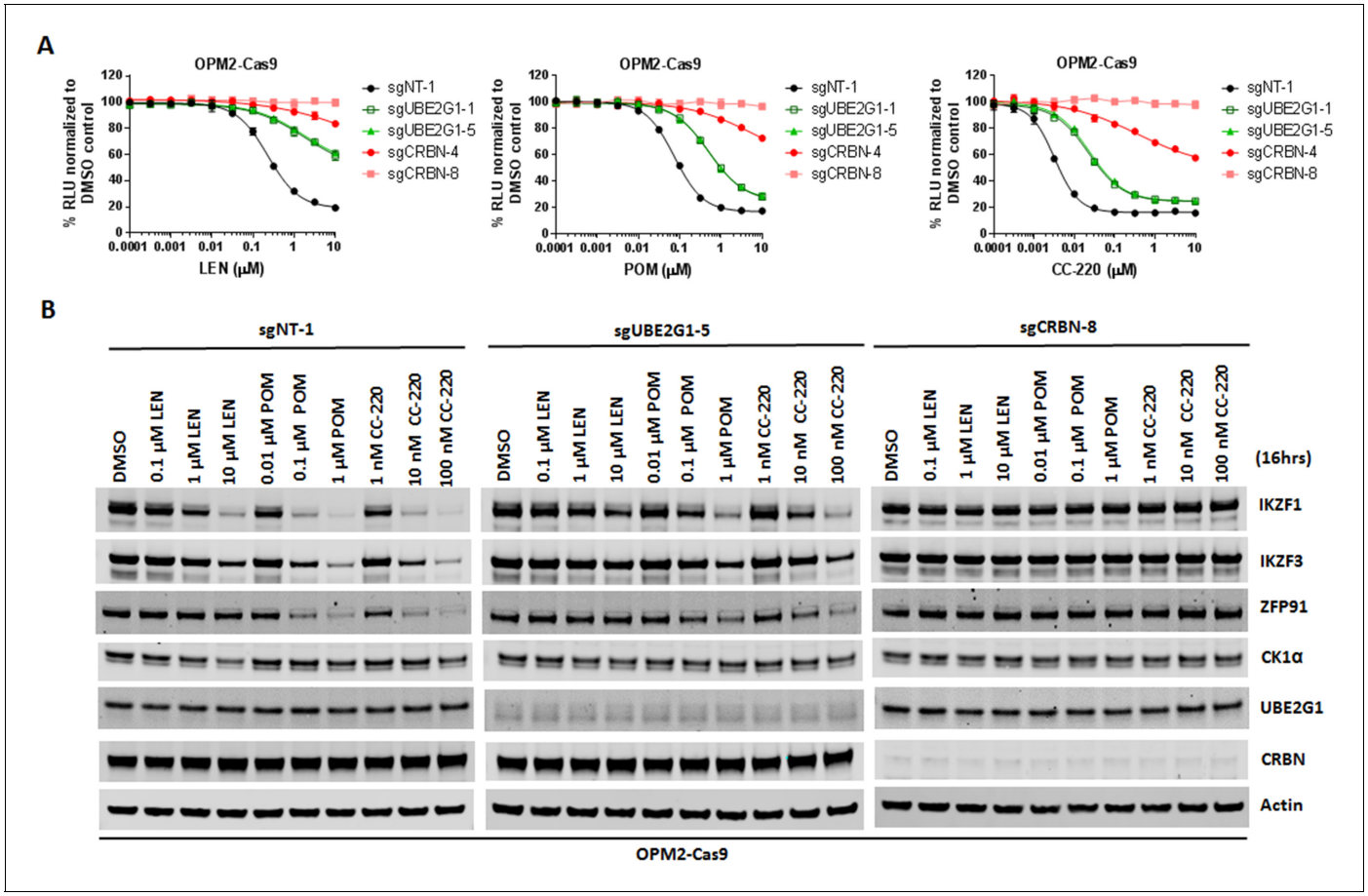

Figure 7. UBE2G1-deficient OPM2 myeloma cells are resistant to lenalidomide and pomalidomide but remain sensitive to CC-220 at clinical relevant concentrations. (**A and B**) Cell proliferation (**A**) and immunoblot analysis (**B**) of OPM2-Cas9 cells transduced with lentiviral vectors expressing non-targeting, *UBE2G1*-specific or *CRBN*-specific sgRNAs. Cells were treated DMSO vehicle control, LEN, POM or CC-220 at the indicated concentrations for 5 days (**A**) or 16 hr (**B**). In (**A**), cell proliferation was determined by CTG, and data are presented as mean ± SD, n = 3 technical replicates. All results shown in this figure are representative of three independent experiments.

DOI: https://doi.org/10.7554/eLife.40958.025

The following source data and figure supplements are available for figure 7:

Source data 1. CTG luminescence signal shown in ***Figure 7A***.

DOI: https://doi.org/10.7554/eLife.40958.028

Figure supplement 1. UBE2G1 knockout diminished the responses to lenalidomide, pomalidomide and CC-220 in myeloma cell lines DF15 and MM1S.

DOI: https://doi.org/10.7554/eLife.40958.026

Figure supplement 1—source data 1. CTG luminescence signal shown in ***Figure 7—figure supplement 1A,C***.

DOI: https://doi.org/10.7554/eLife.40958.027

Although UBE2D3 and UBE2G1 cooperatively regulate the ubiquitination of cereblon neomorphic substrates, ablation of UBE2D3 exhibited very little impact on substrate degradation as compared to loss of UBE2G1, suggesting that additional E2s might fulfill the role of UBE2D3, for example, other UBE2D family proteins with a high degree of sequence homology including UBE2D1/UbcH5a, UBE2D3, and UBE2D4 (***Figure 4—figure supplement 2A***). Indeed, UBE2D1 and UBE2D2 acted synergistically with UBE2G1 in catalyzing the in vitro ubiquitination of GSPT1 in the presence of CC-885, whereas cooperativity among UBE2D1, UBE2D2 and UBE2D3 cannot be detected (***Figure 4—figure supplement 2B***). Knockout of UBE2D1, UBED2 or UBE2D4, however, did not further enhance the inhibition of POM-induced IKZF1 degradation imposed by UBE2G1 knockout in U937 cells (***Figure 2—figure supplement 1C,D,E***). Below we consider various possible explanations for the surprising finding.

First, among all 4 UBE2D family proteins, UBE2D3 is likely the major but not the only E2 utilized by $CRL4^{CRBN}$ to promote neomorphic substrate ubiquitination, possibly owing to their differences in interaction with $CRL4^{CRBN}$, binding affinity with $CRL4^{CRBN}$ or simply relative protein abundance. Knockout of UBE2D3 could potentially remove the gridlock on $CRL4^{CRBN}$, enabling its binding with other UBE2D family proteins which otherwise are much less engaged by $CRL4^{CRBN}$ under physiological conditions. If so, it is not surprising to observe the lack of cooperativity between UBE2G1 and UBE2D1, UBE2D2 or UBE2D4 in promoting IKZF1 degradation in UBE2D3 wild-type cells, as well as the lesser effect of UBE2D3 knockout on IKZF1 degradation than that of UBE2G1 knockout. Second, it is possible that similar to UBE2M/UBC12, UBE2D1, UBE2D2 or UBE2D4 is essential in U937 cells, and therefore only cells with partial inactivation of these three proteins survived after CRISPR knockout, resulting in the underestimation of their involvement in IKZF1 ubiquitination. Third, redundancy among UBE2D1, UBE2D2 and UBE2D4 in replacing the function of UBE2D3 could also prevent the identification of their cooperativity with UBE2G1 by a single gene inactivation approach as used in our screen. Further studies exploiting the combinatorial inactivation of UBE2D3 with one, two or all three remaining UBE2D family proteins will best address this issue. Lastly, we could not rule out the following less satisfying explanations: 1) ineffective gene editing efficiency of the sgRNAs we used to knockout UBE2D1, UBE2D2 and UBE2D4; 2) insufficient assay sensitivity leading to failure in detecting subtle changes of IKZF1 degradation conferred by double knockout of UBE2G1 with less critical E2(s) versus UBE2G1 knockout alone; 3) indirect impact of UBE2D3 inactivation or off-target effect of UBE2D3 sgRNAs on IKZF1 ubiquitination.

It is also interesting to point out that UBE2D3 knockout further blocked the degradation of IKZF1 in UBE2G1 deficient cells (***Figure 2***), whereas the in vitro reconstituted ubiquitination assay clearly suggests that these two enzymes work in sequence (***Figure 4***). Although double knockout of UBE2G1 and UBE2D3 significantly blocked the ubiquitination and degradation of IKZF1 in U937 and 293 T cells (***Figures 2*** and ***5***), this effect is still much less pronounced than that of CRBN knockout (***Figure 1—figure supplement 1***), indicating the existence of additional mechanism(s) modulating IKZF1 degradation. Based on the following observations, we speculate that UBE2D family proteins or other yet-to-be-identified E2(s) could promote the assembly of mixed polyubiquitin chains on cereblon neosubstrates in the absence of UBE2G1, resulting in their ineffective yet significant degradation. First, UBE2D1 and to a lesser extent UBE2D2 are capable of catalyzing CC-885-dependent in vitro polyubiquitination of GSPT1 without the help of UBE2G1 (***Figure 4—figure supplement 2B***, lanes 2, 4 and 6). Second, UBE2D2 knockout impaired the POM-induced degradation of ePL-tagged IKZF1 (***Figure 1—figure supplement 2D***). Third, UBE2D3 overexpression promoted in vivo polyubiquitination of IKZF1 in 293T *UBE2G1-/-; UBE2D3-/-* cells (***Figure 5B***), as well as the degradation of GSPT1 in 293T *UBE2G1-/-* cells (***Figure 4—figure supplement 1B***). Moreover, we might also underappreciate the role of additional ubiquitin chain extending E2(s) that could functionally substitute for UBE2G1. For instance, a UBE2G1 paralog UBE2G2, which was shown to cooperate with UBE2G1 to mediate the polyubiquitination of Cdt1 by $CRL4^{Cdt2}$ (***Shibata et al., 2011***), could play a similar redundant role in coordinating the ubiquitin chain assembly on cereblon neomorphic substrates. However, significant loss of cellular fitness following UBE2G2 knockout in the presence or absence of UBE2G1 in U937 cells could prevent the identification of UBE2G2 in our screen. Further experimentation is again required to explore these hypotheses. Taken together, we postulate that the CM-induced proteolysis of cereblon neomorphic substrates is both redundantly and cooperatively regulated by UBE2D family proteins and UBE2G1/2, with UBE2G1/2 playing a key role in enhancing the rate and extent of K48-linked substrate ubiquitination, resulting in rapid and efficient substrate degradation.

Although loss of UBE2G1 conferred resistance to LEN and POM in human myeloma cell lines, it remains to be seen whether UBE2G1 deficiency occurs in human myeloma patients with inherent or acquired resistance to IMiD drug treatment, especially those with normal cereblon expression. The myeloma cell line SKMM-2, which lost both copies of the *UBE2G1* gene (based on gene copy number characterization in Cancer Cell Line Encyclopedia), and has undetectable UBE2G1 protein expression (***Figure 6B***), was derived from a human myeloma patient who never received any prior treatment with IMiD drugs (***Eton et al., 1989***), warranting the further clinical evaluation of UBE2G1 activity in myeloma patients. Given that UBE2G1 inactivation conferred resistance to all CMs tested and also to cereblon-based PROTACs, patient stratification approaches based on UBE2G1 status might be applicable to the development of IMiD drugs and other novel cereblon modulating agents

for a variety of human diseases. Lastly, CC-220, a novel CM that targets IKZF1 and IKZF3 for degradation much more effectively than does LEN or POM, retained strong antitumor activity at clinically achievable concentrations (***Schafer et al., 2018***) in UBE2G1-deficient myeloma cells, suggesting that human patients with resistance to CM drugs owing to diminished UBE2G1 function may be responsive to next-generation CMs that possess higher efficiency and/or potency for degrading the same target protein.

Materials and methods

Key resources table

Reagent type	Designation	Source or reference	Identifiers	Additional information
Cell line (human)	U937	ATCC	RRID:CVCL_0007	
Cell line (human)	OPM2	DSMZ	RRID:CVCL_1625	
Cell line (human)	293T	Clontech	Cat# 632180	
Antibody	anti-CRBN (rabbit monoclonal antibody)	Celgene	CRBN65	WB (1: 2,000)
Antibody	anti-UBE2G1 (mouse monoclonal antibody)	Santa Cruz Biotechnology	RRID:AB_1130981	WB (1: 500)
Antibody	anti-UBE2D3 (rabbit polyclonal antibody)	Sigma-Aldrich	RRID:AB_10605875	WB (1: 1,000)
Antibody	anti-GSPT1 (rabbit polyclonal antibody)	Abcam	RRID:AB_2115507	WB (1: 1,000)
Antibody	anti-IKZF1 (rabbit monoclonal antibody)	Cell Signaling	RRID:AB_2744523	WB (1: 1,000)
Antibody	anti-IKZF3 (rabbit monoclonal antibody)	Cell Signaling	RRID:AB_2744524	WB (1: 1,000)
Antibody	anti-CK1α(rabbit polyclonal antibody)	Abcam	RRID:AB_10864123	WB (1: 1,000)
Antibody	anti-ZFP91 (rabbit polyclonal antibody)	LifeSpan Biosciences	RRID:AB_2744522	WB (1: 1,000)
Antibody	anti-Cul4A (rabbit polyclonal antibody)	Cell Signaling	RRID:AB_2086563	WB (1: 1,000)
Antibody	anti-DDB1 (rabbit polyclonal antibody)	Cell Signaling	RRID:AB_10634753	WB (1: 1,000)
Antibody	anti-Rbx1 (rabbit polyclonal antibody)	Cell Signaling	RRID:AB_1904121	WB (1: 1,000)
Antibody	anti-HIS (mouse monoclonal antibody)	Qiagen	RRID:AB_2619735	WB (1: 1,000)
Antibody	anti-MBP (mouse monoclonal antibody)	Santa Cruz Biotechnology	RRID:AB_675707	WB (1: 1,000)
Antibody	anti-Actin (mouse monoclonal antibody)	Sigma-Aldrich	RRID:AB_476743	WB (1: 10,000)
Antibody	anti-Tubulin (mouse monoclonal antibody)	Sigma-Aldrich	RRID:AB_477593	WB (1: 10,000)
Recombinant DNA reagent	pcDNA3-8xHIS-Ub (plasmid)	PMID:27338790		transient transfection
Recombinant DNA reagent	plenti-UBC-UBE2G1 -pGK-Pur (plasmid)	this paper		lentiviral transduction
Recombinant DNA reagent	plenti-UBC-UBE2G1 -C90S-pGK-Pur (plasmid)	this paper		lentiviral transduction

Continued on next page

Continued

Reagent type	Designation	Source or reference	Identifiers	Additional information
Recombinant DNA reagent	pRSG16-U6-sgNT-1-UbiC-TagRFP-2A-Puro (plasmid)	this paper		lentiviral transduction
Recombinant DNA reagent	pRSG16-U6-sgCRBN-8-UbiC-TagRFP-2A-Puro (plasmid)	this paper		lentiviral transduction
Recombinant DNA reagent	pRSG16-U6-sgUBE2G1-5-UbiC-TagRFP-2A-Puro (plasmid)	this paper		lentiviral transduction
Recombinant DNA reagent	pRSG16-U6-sgUBE2D3-4-UbiC-TagRFP-2A-Puro (plasmid)	this paper		lentiviral transduction
Chemical compound, drug	MLN4924	Cayman	Cat# 15217	
Chemical compound, drug	MG-132	R and D systems	Cat# 1748/5	
Chemical compound, drug	cycloheximide	EMD	Cat# 239765	
Chemical compound, drug	pomalidomide	Celgene	CC0004047	
Chemical compound, drug	lenalidomide	Celgene	CC0005013	
Chemical compound, drug	CC-885	Celgene	CC0015885	
Chemical compound, drug	CC-220	Celgene	CC0017220	
Commercial assay or kit	HisPur Ni-NTA Magnetic Beads	ThermoFisher	Cat# 88832	
Peptide, recombinant protein	Cul4A-Rbx1	PMID:27338790		Human full length Cul4A and Rbx1
Peptide, recombinant protein	Cereblon-DDB1	PMID:27338790		Human cereblon (amino acids 40–442) and full length human DDB1
Peptide, recombinant protein	MBP-IKZF1	PMID:27338790		IKZF1 (amino acids 140–168)
Peptide, recombinant protein	MBP-GSPT1	PMID:27338790		GSPT1 (amino acids 437–633)
Peptide, recombinant protein	UBE2D1/UbeH5a	R and D systems	Cat# E2-616-100	
Peptide, recombinant protein	UBE2D2/UbeH5b	R and D systems	Cat# E2-622-100	
Peptide, recombinant protein	UBE2D3/UbeH5c	R and D systems	Cat# E2-627-100	
Peptide, recombinant protein	UBE2G1	this paper		Human full length UBE2G1
Peptide, recombinant protein	wild-type Ubiquitin	R and D systems	Cat# U-100H	
Peptide, recombinant protein	K48-only Ubiquitin	R and D systems	Cat# UM-K480-01M	
Peptide, recombinant protein	K48R Ubiquitin	R and D systems	Cat# UM-K48R-01M	
Peptide, recombinant protein	Ube1	R and D systems	Cat# E-305	

Purification of in vitro Ubiquitination Assay Components

Cereblon-DDB1 purification

ZZ-domain-6xHis-thrombin-tagged human cereblon (amino acids 40–442) and full length human DDB1 were co-expressed in SF9 insect cells in ESF921 medium (Expression Systems), in the presence of 50 uM zinc acetate. Cells were resuspended in buffer containing 50 mM Tris-HCl pH 7.5, 500 mM NaCl, 10 mM imidazole, 10% glycerol, 2 mM TCEP, 1X Protease Inhibitor Cocktail (San Diego Bioscience), and 40,000 U Benzonase (Novagen), and sonicated for 30 s. Lysate was clarified by high speed centrifugation at 30,000 rpm for 30 min, and clarified lysate was incubated with Ni-NTA affinity resin (Qiagen) for 1 hr. Complex was eluted with buffer containing 500 mM imidazole, and the ZZ-domain-6xHis tag removed by thrombin cleavage (Enzyme Research) overnight, combined with dialysis in 10 mM imidazole buffer. Cleaved eluate was incubated with Ni-NTA affinity resin (Qiagen), and the flow-through diluted to 200 mM NaCl for further purification over an ANX HiTrap ion exchange column (GE Healthcare). The ANX column was washed with 10 column volumes 50 mM Tris-HCl pH 7.5, 200 mM NaCl, 3 mM TCEP, followed by 10 column volumes of 50 mM Bis-Tris pH 6.0, 200 mM NaCl, 3 mM TCEP, and the cereblon-DDB1 peak eluted at 210 mM NaCl. This peak was collected and further purified by size exclusion chromatography using a Sephacryl S-400 16/60 column (GE Healthcare) in buffer containing 10 mM HEPES pH 7.0, 240 mM NaCl, and 3 mM TECP. The cereblon-DDB1 complex was concentrated to 30 mg/mL.

Cul4A-Rbx1 purification

Human full length Cul4A and Rbx1 were co-expressed in SF9 insect cells. Cells were resuspended in buffer containing 50 mM Tris-HCl pH 7.5, 500 mM NaCl, 10 mM imidazole, 10% glycerol, 2 mM TCEP, 1X Protease Inhibitor Cocktail (San Diego Bioscience), and 40,000 U Benzonase (Novagen), and sonicated for 30 s. Lysate was clarified by high speed centrifugation at 30,000 rpm for 30 min, and clarified lysate was incubated with Ni-NTA affinity resin (Qiagen) for 1 hr. Complex was eluted with buffer containing 500 mM imidazole, and concentrated for size exclusion chromatography. Complex was further purified over an S200 Superdex 200 16/600 column (GE Healthcare) in buffer containing 200 mM NaCl, 50 mM Tris pH 7.5, 3 mM TCEP, and 10% glycerol.

Substrate purification

MBP-IKZF1 (amino acids 140–168) or MBP-GSPT1 (amino acids 437–633) was expressed in *E.coli* BL21 (DE3) Star cells (Life Technologies) using 2XYT media (Teknova). Cells were induced at OD_{600} 0.6 for 18 hr at 16 ˚C, with 150 uM zinc acetate added upon induction for IKZF1 expression. Cells were pelleted and resuspended in buffer containing 200 mM NaCl, 50 mM Tris pH 7.5, 3 mM TCEP, 10% glycerol, 150 µM zinc acetate, 0.01 mg/mL lysozyme (Sigma), 40,000 U benzonase (Novagen), and 1X protease inhibitor cocktail (San Diego Bioscience). Resuspended cells were frozen, thawed for purification, and sonicated for 30 s before high speed centrifugation at 30,000 rpm for 30 min. Clarified lysate was incubated with maltose affinity resin (NEB) at 4 ˚C for 1 hr before beads were washed. Protein was eluted with buffer containing 200 mM NaCl, 50 mM Tris pH 7.5, 3 mM TCEP, 10% glycerol, 150 µM zinc acetate, and 10 mM maltose. Eluate was concentrated and further purified by size exclusion chromatography over a Superdex 200 16/600 column (GE Healthcare) in buffer containing 200 mM NaCl, 50 mM Tris pH 7.5, 3 mM TCEP, 10% glycerol, and 150 µM zinc acetate.

UBE2G1 purification from *E. coli*

Human full length UBE2G1 with an N-terminal 6XHis-thrombin tag was expressed in *E.coli* BL21 (DE3) Star cells (Life Technologies) using 2XYT media (Teknova). Cells were induced at OD_{600} 0.6 for 18 hr at 16 ˚C. Cells were pelleted and resuspended in buffer containing 50 mM Tris pH7.5, 250 mM NaCl, 3 mM TCEP, 1X Protease Inhibitor Cocktail (San Diego Bioscience), 20 mM imidazole, and 40,000 U Benzonase (Novagen), and sonicated for 3 times for 30 s. Lysate was clarified by high speed centrifugation at 30,000 rpm for 30 min, and clarified lysate was incubated with Ni-NTA affinity resin (Qiagen) for 1 hr at 4C. The protein was eluted with buffer containing 500 mM imidazole. The 6XHis tag was then removed by thrombin cleavage (Enzyme Research) overnight, combined with dialysis into 50 mM Tris pH7.5, 250 mM NaCl, 3 mM TCEP, 1X Protease Inhibitor Cocktail (San Diego Bioscience), 20 mM imidazole. The cleaved protein was then loaded onto a 5 ml HiTrap Ni column (GE Healthcare), and cleaved protein collected in the flow-through. The flow-through was

then concentrated and further purified by size exclusion chromatography over a Superdex 75 16/600 column (GE Healthcare) in buffer containing 20 mM Tris pH7.5, 150 mM NaCl, 1 mM DTT, and concentrated to 25 µM.

E2 purification from 293 T cells

FLAG tagged UBE2D3 wild-type and C85S mutant, and FLAG-tagged UBE2G1 wild-type and C905S mutant were purified from 293T *UBE2G1-/-* cell lines stably expressing the respective protein. A pellet of ~5000 million cells expressing a FLAG-tagged E2 was re-suspended in buffer containing 50 mM Tris-HCl pH 7.5, 250 mM NaCl, 1 mM TCEP, 1X Protease Inhibitor Cocktail (San Diego Bioscience), and Phosphatase inhibitor cocktail (Sigma (Roche), REF 04 906 837 001), and sonicated for 15 s. Lysate was clarified by high speed centrifugation at 30,000 rpm for 30 min, and clarified lysate was incubated with anti-FLAG M2 Affinity Gel (A2220 Sigma) for 2 hr. The E2 was eluted with buffer containing 50 mM Tris pH7.5, 250 mM NaCl, 0.15 mg/ml FLAG peptide (3X FLAG Peptide F4799, Sigma Aldrich). The protein was then dialyzed into 4 L of buffer containing 50 mM Tris pH 7.5 and 250 mM NaCl for one hour twice. The protein was then concentrated and further purified by size exclusion chromatography over a Superdex 75 16/600 column (GE Healthcare) in buffer containing 20 mM Tris pH 7.5, 150 mM NaCl. All four proteins were then concentrated to 25 µM final concentration.

In vitro ubiquitination assays

Purified E1, E2, ubiquitin, Cul4A-Rbx1, and cereblon-DDB1 proteins were used to reconstitute the ubiquitination of MBP-fused GSPT1 or IKZF1 substrates in vitro. Purified recombinant human Ube1 E1 (E-305), UbcH5a/UBE2D1 (E2-616-100), UbcH5b/UBE2D2 (E2-622-100), UbcH5c/UBE2D3 (E2-627-100), wild-type ubiquitin (U-100H), K48R ubiquitin (UM-K48R-01M), and K48-only ubiquitin (UM-K480-01M) were purchased from R and D systems. For the ubiquitination of IKZF1 or GSPT1 shown in ***Figure 4A and B***, and ***Figure 4—figure supplements 1C*** and ***2B***, reaction components were mixed to final concentrations of 80 mM ATP, 1.5 µM Ube1, 275 µM Ub, 2 µM Cul4-Rbx1, 2 µM cereblon-DDB1, 5 uM IKZF1 (a.a. 140–168) or 5 µM MBP-GSPT1 (a.a. 437–633) as indicated, and then 5 µM UBE2D1, 5 µM UBE2D2, 5 µM UBE2D3 (purified from either from E.coli or human cells), or 7.5 µM UBE2G1 (purified from either from E.coli or human cells), was added alone or in combination, as indicated. Reactions were incubated in the presence of either DMSO or 80 µM compound (pomalidomide or CC-885) in ubiquitination assay buffer (20 mM HEPES pH 7.5, 150 mM NaCl, 10 mM $MgCl_2$). To start the reactions, E1, E2, ATP and ubiquitin were pre-incubated for 30 min, and separately MBP-substrate, CRBN-DDB1, Cul4-Rbx1, and compound were pre-incubated for 5 min at room temperature, before ubiquitination reactions were started by mixing the two pre-incubations. Reactions were incubated at 30˚C for 2 hr before separation by SDS-PAGE followed by immunoblot analysis using anti-MBP antibody (MBP-probe R29.6, Santa Cruz). For the ubiquitin mutant reactions shown in ***Figures 4C, D***, 275 µM K48-only or K48R ubiquitin was substituted for wild-type ubiquitin as indicated, and the E. coli-purified UBE2G1 was used. Reactions were incubated at 30˚C for 2 hr before separation by SDS-PAGE followed by immunoblot analysis using anti-MBP antibody (MBP-probe R3.2, Santa Cruz).

For the ubiquitination of a pre-ubiquitinated substrate shown in ***Figure 4E***, MBP-GSPT1 (a.a. 437–633) was incubated with 80 mM ATP, 3 µM Ube1, 600 µM Ub, 4 µM Cul4-Rbx1, 4 µM cereblon-DDB1, 5 µM UBE2D3 (purified from E. coli), and 80 uM CC-885 for 4 hr before separation of the reaction over a 10/300 S200 GL (GE 17-5175-01) size exclusion chromatography column to separate the substrate from the rest of the ubiquitination reaction components. 1.25 µM purified MBP-GSPT1 was then used as the substate in ubiquitnation reactions including 80 mM ATP, 1.5 µM Ube1, 600 µM Ub, 2 µM Cul4-Rbx1, 2 µM cereblon-DDB1, 80 µM CC-885, and 7 µM UBE2G1 (purified from E. coli). Reactions were incubated at 30˚C for 2 hr before separation by SDS-PAGE followed by immunoblot analysis using anti-MBP antibody (MBP-probe R29.6, Santa Cruz).

Cell culture and materials

Human embryonic kidney cell line 293T (Clontech) was maintained in Dulbecco's Modified Eagle's medium (DMEM; Invitrogen) supplemented with 10% fetal bovine serum (FBS; Invitrogen), 1x sodium pyruvate (Invitrogen), 1x non-essential amino acids (Invitrogen), 100 U/mL penicillin (Invitrogen), and 100 µg/mL streptomycin (Invitrogen). Acute myeloid leukemia cell lines U937, MOLM-13,

and MV4-11 and myeloma cell line MM1S were purchased from American Tissue Culture Collection (ATCC). Acute myeloid leukemia cell line OCI-AML2 cell line and myeloma cell lines OPM2 was purchased from Deutsche Sammlung von Mikroorganismen und Zellkulturen GmbH (DSMZ). Myeloma cell line DF15 was obtained from Dr John Shaughnessy (University of Arkansas, Little Rock, AR, USA). U937, MOLM-13, OPM2, MM1S and DF15 cell lines were maintained in Roswell Park Memorial Institute (RPMI) 1640 tissue culture medium (Invitrogen) supplemented with 10% FBS, 1x sodium pyruvate, 1x non-essential amino acids, 100 U/mL penicillin, and 100 µg/mL streptomycin. MV4-11 cell line was maintained in Iscove's Modified Dulbecco's medium (IMDM; (Invitrogen) supplemented with 10% FBS, 1x sodium pyruvate, 1x non-essential amino acids, 100 U/mL penicillin, and 100 µg/mL streptomycin. OCI-AML2 cell line was maintained in minimal essential medium (MEM; Invitrogen) supplemented with 10% FBS, 1x sodium pyruvate, 1x non-essential amino acid, 100 U/mL penicillin, and 100 µg/mL streptomycin. All cell lines were cultured at 37˚C with 5% CO_2 in the relevant media mentioned above. All cell lines were authenticated by autosomal STR profiling. All cell lines were tested routinely using the MycoAlert Mycoplasma Detection Kit (Lonza), and confirmed mycoplasma-negative.

Plasmids

UBE2G1 and UBE2D3 complimentary deoxyribonucleic acid (cDNA) clones were purchased from Dharmacon. The coding regions of UBE2G1 and UBE2D3 were polymerase chain reaction (PCR)-amplified and shuttled into pDONR223 via BP (attB and attP) recombination to generate pDONR223-UBE2G1, pDONR223-FLAG-UBE2G1, and pDONR223-FLAG-UBE2D3. Site-directed mutagenesis using overlapping PCR was then carried out to generate pDONR223-UBE2G1-CR (CRISPR resistant), pDONR223-UBE2G1-C90S-CR, pDONR223-FLAG-UBE2G1-CR, and pDONR223-FLAG-UBE2G1-C90S-CR, and pDONR223-FLAG-UBE2D3-C85S. Next, gateway donor vectors pDONR223-UBE2G1-CR and pDONR223-UBE2G1-C90S-CR were shuttled into plenti-Ubcp-gateway-IRES-Pur or plenti-PGK-gateway-IRES-Pur via LR (attL and attR) recombination to generate plenti-Ubcp-UBE2G1-CR-IRES-Pur, plenti-Ubcp-UBE2G1-C90S-CR-IRES-Pur, plenti-PGK-UBE2G1-CR-IRES-Pur, and plenti-PGK-UBE2G1-C90S-CR-IRES-Pur. Gateway donor vectors pDONR223-FLAG-UBE2G1-CR, pDONR223-FLAG-UBE2G1-C90S-CR, pDONR223-FLAG-UBE2D3, and pDONR223-FLAG-UBE2D3-C85S were shuttled into plenti-EF1α-gateway-IRES-Pur via LR recombination to generate plenti-EF1α-FLAG-UBE2G1-CR-IRES-Pur, plenti-EF1α-FLAG-UBE2G1-C90S-CR-IRES-Pur, plenti-EF1α-FLAG-UBE2D3-IRES-Pur, and plenti-EF1α-FLAG-UBE2D3-C85S-IRES-Pur. Constructs pDONR221-U6-sgRNA-EF1a-Cas9-P2A-GFP, plenti-EF1α-Cas9-IRES-Bla, pDONR223-IKZF1, pcDNA3-IKZF1-V5, pcDNA3-CRBN, and pcDNA3-8xHis-Ub were described previously (***Matyskiela et al., 2016***; ***Hagner et al., 2015***). The Cas9-P2A-GFP coding region of pDONR221-U6-sgRNA-EF1a-Cas9-P2A-GFP was subcloned into pcDNA3.1 (Invitrogen) to generate pcDNA3.1-Cas9-P2A-GFP. The IKZF1 coding region of pDONR223-IKZF1 was shuttle into plenti-EF1α-ePL-gateway-IRES-Bla via LR recombination to generate plenti-EF1α-ePL-IKZF1-IRES-Bla. Complementary oligonucleotides containing three non-targeting sgRNAs or three gene-specific sgRNAs targeting CRBN or each of the 41 annotated E2 enzymes were annealed and cloned into pRSG16-U6-sgEV-UbiC-TagRFP-2A-Puro or pRSG16-U6-sgEV-UbiC-Hyg, both of which were modified from pRSG16-U6-sg-HTS6C-UbiC-TagRFP-2A-Puro (Cellecta). All sgRNA sequences used in this report (see ***Supplementary file 1***) were selected from the human genome-wide CRISPR sgRNA library (Cellecta).

Lentiviral production and transduction

Lentiviral plasmid was cotransfected with the 2nd Generation packaging system (ABM) into 293 T cells (Clontech) using Lipofectamine 2000. After 16 hr of incubation, media was changed to fresh DMEM media supplemented with 20% FBS. At 48 hr post transfection, viral supernatant was collected and cleared via centrifugation at 2000 rpm for 5 min, and then filtered through a 0.45 micron cellulose acetate or nylon filter unit. Acute myeloid leukemia and myeloma cell lines were spin-inoculated with lentivirus at 2500 rpm for 120 min. After twelve hours, viral supernatant was removed and complete culture media was added to the cells. Forty-eight hours later, cells were incubated with 1 ~ 2 µg/mL puromycin (Thermofisher), 10 ~ 20 µg/mL blasticidin (Thermofisher), or 250 ~ 500 µg/

mL hygromycin B (Thermofisher) for an additional 2 ~ 7 days to select cells stably integrated with lentiviral vectors.

CRISPR gene editing

AML and MM cell lines were transduced with plenti-EF1a-Cas9-IRES-Bla, followed by limiting dilution and blasticidin selection in 96-well plates (Corining) to generate single clones stably expressing Cas9. The expression of Cas9 in stable clones were validated by immunoblot analysis. Next, Cas9-expressing cells were transduced with pRSG16-U6-sgNT-1-UbiC-TagRFP-2A-Puro, pRSG16-U6-sgNT-3-UbiC-TagRFP-2A-Puro, pRSG16-U6-sgUBE2G1-1-UbiC-TagRFP-2A-Puro, pRSG16-U6-sgUBE2G1-5-UbiC-TagRFP-2A-Puro, pRSG16-U6-sgUBE2D3-4-UbiC-TagRFP-2A-Puro, or pRSG16-U6-sgCRBN-8-UbiC-TagRFP-2A-Puro. One days after transduction, cells were selection with puromycin for 2 days. Then, gene editing efficiency was verified by immunoblot analysis with antibodies recognizing the targeted proteins. For gene editing of both UBE2G1 and UBE2D3, U937-Cas9 cells were first transduced with pRSG16-U6-sgUBE2G1-5-UbiC-Hyg. After 24 hr, cells were selected with hygromycin B selection for additional 5 days, and then transduced with pRSG16-U6-sgUBE2D3-4-UbiC-TagRFP-2A-Puro, followed by puromycin selection for 2 days and immunoblot analysis.

293 T cells were transiently transfected with pcDNA3.1-Cas9-P2A-GFP, pRSG16-U6-sgUBE2G1-5-UbiC-TagRFP-2A-Puro with or without pRSG16-U6-sgUBE2D3-4-UbiC-TagRFP-2A-Puro. Three days after transfection, cells were subjected to limiting dilution into 96-well plates. After two weeks, stable clones were cherry-picked, expanded and subjected to immunoblot analysis. 293T *UBE2G1-/-* clone 13 was validated to be UBE2G1 deficient, and *UBE2G1-/-;UBE2D3-/-* clone 4 was proven deficient for both UBE2G1 and UBE2D3.

For the single-guide RNA directed E2 CRISPR screen, U937 Cas9 cells were first transduced with plenti-EF1a-ePL-IKZF1-IRES-Bla to generate U937_Cas9_ePL-IKZF1 cells, which were then transduced with the focused lentiviral CRISPR library containing three non-targeting control sgRNAs and three gene-specific sgRNAs targeting each of the 41 E2 enzymes.

For the dual-guide RNA directed E2 CRISPR screen, U937_Cas9_ePL-IKZF1 were transduced with pRSG16-U6-sgUBE2G1-5-UbiC-Hyg, followed by hygromycin B selection for additional 5 days. Then, cells were transduced with the focused lentiviral CRISPR library targeting all annotated E2s as described above.

IKZF1-ePL degradation assay

Four days after transduction with lentiviral vectors expressing non-targeting, *CRBN*-specific or *UBE2*-specific sgRNA, U937_Cas9_ePL-IKZF1 cells were dispensed into a 384-well plate (Corning) pre-spotted with pomalidomide at varying concentrations. Twenty-five microliters of RPMI-1640 growth media containing 5000 cells was dispensed into each well. After incubation at 37°C with 5% CO_2 for 16 hr, 25 µL of the InCELL Hunter Detection Reagent Working Solution (DiscoverX) was added to each well and incubated at RT for 30 min protected from light. After 30 min, luminescence was read on an EnVision Multimode Plate Reader (Perkin Elmer). For each cell line, The IKZF1 degradation induced by pomalidomide at each indicated concentration was normalized with the DMSO control. Then, a four parameter logistic model (sigmoidal dose-response model) was used to plot the IKZF1 destruction curves. All percentage of control IKZF1 destruction curves were processed and graphed using GraphPad Prism Version 7. To assess the effect of single knockout of a given UBE2 gene on pomalidomide-induced IKZF1 degradation as shown ***Figure 1B*** and ***Figure 1—figure supplement 2***, an unpaired two-sided t-test was used to compare the difference between sgUBE2 and parental control. To assess the effect of dual knockout of UBE2G1 and a given UBE2 gene as shown in ***Figure 2B*** and ***Figure 2—figure supplement 1***, an unpaired two-sided t-test was used to compare the difference between sgUBE2G1 alone versus sgUBE2G1 plus sgUBE2. $p<0.05$ is considered as significant.

Cell proliferation assay

AML cell lines (5000 cells per well), MM cell lines (5000 cells per well) or 293 T cells (2000 cells per well) in 50 µL complete culture media were seeded into black 384-well plates containing with DMSO or test compounds. After 3 or 5 days, cell proliferation was assessed using CTG according to manufacturer's instructions. Relative cell proliferation was normalized against the DMSO control. The

growth inhibitory curve of each test compound was processed and graphed using GraphPad Prism Version 7. $p<0.05$, unpaired two-sided t-test, is considered as significant.

Immunoblot analysis

Following treatment with test compounds at 37°C for the indicated time, cells were washed in ice-cold 1X PBS twice before harvest in Buffer A [50 mM Tris.Cl (pH 7.6), 150 mM NaCl, 1% Triton X-100, 1 mM EDTA, 1 mM EGTA, 1 mM β-glycerophosphate, 2.5 mM sodium pyrophosphate, 1 mM Na3VO4, 1 µg/mL leupeptin, one tablet of Complete ULTRA protease inhibitor cocktail (Roche), and one tablet of PhosSTOP phosphatase inhibitor cocktail (Roche)]. Whole cell extracts were collected after centrifugation at top speed for 10 min, resolved by SDS-PAGE gel electrophoresis, transferred onto a nitrocellulose membrane using the Turboblot system (Bio-Rad), and probed with the indicated primary antibodies. Bound antibodies were detected with IRDye-680 or −800 conjugated secondary antibodies using a LI-COR scanner.

Protein half life analysis

293T parental and *UBE2G1-/-* cells were pretreated with DMSO or pomalidomide (1 µM) for 30 min, followed by the addition of 100 µg/ml cycloheximide (EMD) into the culture medium. At various time points as indicated in ***Figure 3D***, cells were collected and subjected to immunoblot analysis.

In vivo ubiquitination assay

The ubiquitination assays were carried out as described previously (***Lu et al., 2014b***). In brief, 293T parental, *UBE2G1-/-*, and *UBE2G1-/-;UBE2D3-/-* cells seeded in six well plates were transiently transfected with pcDNA3-IKZF1-V5, pcDNA3- CRBN, pcDNA3-8 x His-Ub, or pcDNA3 empty vector. In ***Figure 5B and C*** and ***Figure 5—figure supplements 1B,C***, 293T *UBE2G1-/-* and *UBE2G1-/-; UBE2D3-/-* cells were also transfected with plenti-EF1a-UBE2G1-IRES-Pur, plenti-EF1a-UBE2D3-IRES-Pur or both. Forty-eight hours post transfection, cells were treated with 10 µM MG-132 (R and D systems) with or without an increased concentrations of pomalidomide as indicated. Eight hours later, cells were washed twice with ice cold PBS and resuspended in 1 mL PBS. Twenty uL of the cell suspension was boiled in LDS loading buffer, and the remaining cells were collected via centrifugation and lysed in Buffer C (6M guanidine-HCL, 0.1M Na2HPO4/NaH2PO4, 20 mM imidazole, pH 8.0). Next, whole cell extracts were sonicated for 12 pulses, and mixed with 20 µL of HisPur Ni-NTA Magnetic Beads (Thermofisher) at 37°C for 4 hr. Ni-NTA beads were then washed three times with Buffer C, three times with Buffer D (1 vol of Buffer C: 3 volumes of Buffer E), and three times with Buffer E (25 mM Tris.CL, 20 mM imidazole, pH 6.8). Bound proteins were eluted by boiling in 2x LDS loading buffer and subjected to immunoblot analysis.

Antibodies

Rabbit anti-human CRBN65 monoclonal antibody (mAb) (Celgene, San Diego, CA); rabbit anti-human GSPT1 polyclonal antibody (pAb; Abcam, #ab49878), rabbit anti-human IKZF1 mAb (Cell Signaling, #14859), rabbit anti-human IKZF3 mAb (Cell Signaling, #15103), rabbit anti-human CK1α pAb (Abcam, #ab108296), rabbit anti-human ZFP91 pAb (LifeSpan Biosciences, #LS-B14788), mouse anti-human UBE2G1 mAb (Santa Cruz, #SC-100619), rabbit anti-human UBE2G1 pAb (Abcam, #SC-101371), mouse anti-human UBE2D3 mAb (Abcam, #ab58251), rabbit anti-human UBE2D3 pAb (Sigma, #SAB2102622), rabbit anti-human Cul4A pAb (Cell Signaling, #2699), rabbit anti-human DDB1 pAb (Cell Signaling, #5428), rabbit anti-human Rbx1 pAb (Cell Signaling, #4397), rabbit anti-human Cdt1 mAb (Cell Signaling, #8064), rabbit anti-human Cdt2 pAb (Cell Signaling, #A300-948A), rabbit anti-human Set8 pAb (Cell Signaling, #2996), rabbit anti-human RBM39 pAb (Sigma, #HPA001591), rabbit anti-human p21 mAb (Cell Signaling, #2947), rabbit anti-human p27 mAb (Cell Signaling, #3686), rabbit anti-human c-Myc mAb (Cell Signaling, #5605), rabbit anti-human BRD4 pAb (Abcam, #ab128874), mouse anti-penta-HIS mAb (Qiagen, #34660), mouse anti-human Actin mAb (Sigma, #A5316) and mouse anti-human Tubulin mAb (Sigma, #T9026)(Sigma) were used as primary antibodies. Goat anti-mouse 800 antibody (LICOR Biosciences), goat anti-rabbit 680 antibody (LICOR Biosciences), goat anti-mouse 800 antibody (LICOR Biosciences) and goat anti-rabbit 680 antibody (LI-COR Biosciences) were used as secondary antibodies.

Acknowledgements

The authors thank members of the early drug discovery team at Celgene for helpful discussion and technical support.

Additional information

Competing interests

Gang Lu, Stephanie Weng, Mary Matyskiela, Xinde Zheng, Wei Fang, Scott Wood, Christine Surka, Reina Mizukoshi, Chin-Chun Lu, Derek Mendy, In Sock Jang, Kai Wang, Mathieu Marella, Suzana Couto, Brian Cathers, James Carmichael, Philip Chamberlain, Mark Rolfe: Employee of Celgene.

Funding

No external funding was received for this work

Author contributions

Gang Lu, Conceptualization, Data curation, Formal analysis, Supervision, Validation, Investigation, Visualization, Methodology, Writing—original draft, Project administration, Writing—review and editing; Stephanie Weng, Xinde Zheng, Data curation, Investigation, Methodology, Writing—review and editing; Mary Matyskiela, Conceptualization, Methodology, Writing—review and editing; Wei Fang, Data curation, Investigation, Visualization, Methodology, Writing—review and editing; Scott Wood, Chin-Chun Lu, Data curation, Validation, Investigation, Writing—review and editing; Christine Surka, Derek Mendy, Mathieu Marella, Data curation, Investigation, Writing—review and editing; Reina Mizukoshi, Data curation, Validation, Writing—review and editing; In Sock Jang, Investigation, Methodology, Writing—review and editing; Kai Wang, Supervision, Investigation, Writing—review and editing; Suzana Couto, Data curation, Supervision, Investigation; Brian Cathers, Resources, Project administration, Writing—review and editing; James Carmichael, Philip Chamberlain, Resources, Supervision, Writing—review and editing; Mark Rolfe, Conceptualization, Resources, Supervision, Project administration, Writing—review and editing

Author ORCIDs

Gang Lu http://orcid.org/0000-0002-2138-1522

Decision letter and Author response

Decision letter https://doi.org/10.7554/eLife.40958.032
Author response https://doi.org/10.7554/eLife.40958.033

Additional files

Supplementary files

- Supplementary file 1. Sequences of non-targeting and gene-specific guide RNAs used in this manuscript.

DOI: https://doi.org/10.7554/eLife.40958.029

- Transparent reporting form

DOI: https://doi.org/10.7554/eLife.40958.030

Data availability

All data generated or analysed during this study are included in the manuscript and supporting files

References

Blondel M, Galan JM, Chi Y, Lafourcade C, Longaretti C, Deshaies RJ, Peter M. 2000. Nuclear-specific degradation of Far1 is controlled by the localization of the F-box protein Cdc4. *The EMBO Journal* **19**:6085–6097. DOI: https://doi.org/10.1093/emboj/19.22.6085, PMID: 11080155

Bondeson DP, Crews CM. 2017. Targeted protein degradation by small molecules. *Annual Review of Pharmacology and Toxicology* **57**:107–123. DOI: https://doi.org/10.1146/annurev-pharmtox-010715-103507, PMID: 27732798

Chamberlain PP, Lopez-Girona A, Miller K, Carmel G, Pagarigan B, Chie-Leon B, Rychak E, Corral LG, Ren YJ, Wang M, Riley M, Delker SL, Ito T, Ando H, Mori T, Hirano Y, Handa H, Hakoshima T, Daniel TO, Cathers BE. 2014. Structure of the human Cereblon-DDB1-lenalidomide complex reveals basis for responsiveness to thalidomide analogs. *Nature Structural & Molecular Biology* **21**:803–809. DOI: https://doi.org/10.1038/nsmb.2874, PMID: 25108355

Choi YS, Lee YJ, Lee SY, Shi L, Ha JH, Cheong HK, Cheong C, Cohen RE, Ryu KS. 2015. Differential ubiquitin binding by the acidic loops of Ube2g1 and Ube2r1 enzymes distinguishes their Lys-48-ubiquitylation activities. *Journal of Biological Chemistry* **290**:2251–2263. DOI: https://doi.org/10.1074/jbc.M114.624809, PMID: 25471371

Deshaies RJ. 2015. Protein degradation: Prime time for PROTACs. *Nature chemical biology* **11**:634–635. DOI: https://doi.org/10.1038/nchembio.1887, PMID: 26284668

Eton O, Scheinberg DA, Houghton AN. 1989. Establishment and characterization of two human myeloma cell lines secreting kappa light chains. *Leukemia* **3**:729–735. PMID: 2506399

Feldman RM, Correll CC, Kaplan KB, Deshaies RJ. 1997. A complex of Cdc4p, Skp1p, and Cdc53p/cullin catalyzes ubiquitination of the phosphorylated CDK inhibitor Sic1p. *Cell* **91**:221–230. DOI: https://doi.org/10.1016/S0092-8674(00)80404-3, PMID: 9346239

Fischer ES, Böhm K, Lydeard JR, Yang H, Stadler MB, Cavadini S, Nagel J, Serluca F, Acker V, Lingaraju GM, Tichkule RB, Schebesta M, Forrester WC, Schirle M, Hassiepen U, Ottl J, Hild M, Beckwith RE, Harper JW, Jenkins JL, et al. 2014. Structure of the DDB1-CRBN E3 ubiquitin ligase in complex with thalidomide. *Nature* **512**:49–53. DOI: https://doi.org/10.1038/nature13527, PMID: 25043012

Gandhi AK, Kang J, Havens CG, Conklin T, Ning Y, Wu L, Ito T, Ando H, Waldman MF, Thakurta A, Klippel A, Handa H, Daniel TO, Schafer PH, Chopra R. 2014. Immunomodulatory agents lenalidomide and pomalidomide co-stimulate T cells by inducing degradation of T cell repressors Ikaros and Aiolos via modulation of the E3 ubiquitin ligase complex CRL4(CRBN.). *British Journal of Haematology* **164**:811–821. DOI: https://doi.org/10.1111/bjh.12708, PMID: 24328678

Gong L, Yeh ET. 1999. Identification of the activating and conjugating enzymes of the NEDD8 conjugation pathway. *Journal of Biological Chemistry* **274**:12036–12042. DOI: https://doi.org/10.1074/jbc.274.17.12036, PMID: 10207026

Hagner PR, Man H-W, Fontanillo C, Wang M, Couto S, Breider M, Bjorklund C, Havens CG, Lu G, Rychak E, Raymon H, Narla RK, Barnes L, Khambatta G, Chiu H, Kosek J, Kang J, Amantangelo MD, Waldman M, Lopez-Girona A, et al. 2015. CC-122, a pleiotropic pathway modifier, mimics an interferon response and has antitumor activity in DLBCL. *Blood* **126**:779–789. DOI: https://doi.org/10.1182/blood-2015-02-628669

Harousseau JL, Attal M. 2017. How I treat first relapse of myeloma. *Blood* **130**:963–973. DOI: https://doi.org/10.1182/blood-2017-03-726703, PMID: 28679737

Hershko A, Ciechanover A. 1998. The ubiquitin system. *Annual Review of Biochemistry* **67**:425–479. DOI: https://doi.org/10.1146/annurev.biochem.67.1.425, PMID: 9759494

Huang X, Dixit VM. 2016. Drugging the undruggables: exploring the ubiquitin system for drug development. *Cell Research* **26**:484–498. DOI: https://doi.org/10.1038/cr.2016.31, PMID: 27002218

Jang SW, Elsasser S, Campbell JL, Kim J. 2001. Identification of Cdc6 protein domains involved in interaction with Mcm2 protein and Cdc4 protein in budding yeast cells. *Biochemical Journal* **354**:655–661. DOI: https://doi.org/10.1042/bj3540655, PMID: 11237870

Jin L, Williamson A, Banerjee S, Philipp I, Rape M. 2008. Mechanism of ubiquitin-chain formation by the human anaphase-promoting complex. *Cell* **133**:653–665. DOI: https://doi.org/10.1016/j.cell.2008.04.012, PMID: 18485873

Kleiger G, Deshaies R. 2016. Tag team ubiquitin ligases. *Cell* **166**:1080–1081. DOI: https://doi.org/10.1016/j.cell.2016.08.014, PMID: 27565338

Komander D, Rape M. 2012. The ubiquitin code. *Annual Review of Biochemistry* **81**:203–229. DOI: https://doi.org/10.1146/annurev-biochem-060310-170328, PMID: 22524316

Kortüm KM, Mai EK, Hanafiah NH, Shi CX, Zhu YX, Bruins L, Barrio S, Jedlowski P, Merz M, Xu J, Stewart RA, Andrulis M, Jauch A, Hillengass J, Goldschmidt H, Bergsagel PL, Braggio E, Stewart AK, Raab MS. 2016. Targeted sequencing of refractory myeloma reveals a high incidence of mutations in CRBN and Ras pathway genes. *Blood* **128**:1226–1233. DOI: https://doi.org/10.1182/blood-2016-02-698092, PMID: 27458004

Krönke J, Udeshi ND, Narla A, Grauman P, Hurst SN, McConkey M, Svinkina T, Heckl D, Comer E, Li X, Ciarlo C, Hartman E, Munshi N, Schenone M, Schreiber SL, Carr SA, Ebert BL. 2014. Lenalidomide causes selective degradation of IKZF1 and IKZF3 in multiple myeloma cells. *Science* **343**:301–305. DOI: https://doi.org/10.1126/science.1244851, PMID: 24292625

Krönke J, Fink EC, Hollenbach PW, MacBeth KJ, Hurst SN, Udeshi ND, Chamberlain PP, Mani DR, Man HW, Gandhi AK, Svinkina T, Schneider RK, McConkey M, Järås M, Griffiths E, Wetzler M, Bullinger L, Cathers BE, Carr SA, Chopra R, et al. 2015. Lenalidomide induces ubiquitination and degradation of CK1α in del(5q) MDS. *Nature* **523**:183–188. DOI: https://doi.org/10.1038/nature14610, PMID: 26131937

Lebraud H, Heightman TD. 2017. Protein degradation: a validated therapeutic strategy with exciting prospects. *Essays In Biochemistry* **61**:517–527. DOI: https://doi.org/10.1042/EBC20170030, PMID: 28970340

Lehti M, Donelan E, Abplanalp W, Al-Massadi O, Habegger KM, Weber J, Ress C, Mansfeld J, Somvanshi S, Trivedi C, Keuper M, Ograjsek T, Striese C, Cucuruz S, Pfluger PT, Krishna R, Gordon SM, Silva RA, Luquet S,

Castel J, et al. 2013. High-density lipoprotein maintains skeletal muscle function by modulating cellular respiration in mice. *Circulation* **128**:2364–2371. DOI: https://doi.org/10.1161/CIRCULATIONAHA.113.001551, PMID: 24170386

Li W, Tu D, Brunger AT, Ye Y. 2007. A ubiquitin ligase transfers preformed polyubiquitin chains from a conjugating enzyme to a substrate. *Nature* **446**:333–337. DOI: https://doi.org/10.1038/nature05542, PMID: 17310145

Lu G, Middleton RE, Sun H, Naniong M, Ott CJ, Mitsiades CS, Wong KK, Bradner JE, Kaelin WG. 2014a. The myeloma drug lenalidomide promotes the cereblon-dependent destruction of ikaros proteins. *Science* **343**: 305–309. DOI: https://doi.org/10.1126/science.1244917, PMID: 24292623

Lu G, Zhang Q, Huang Y, Song J, Tomaino R, Ehrenberger T, Lim E, Liu W, Bronson RT, Bowden M, Brock J, Krop IE, Dillon DA, Gygi SP, Mills GB, Richardson AL, Signoretti S, Yaffe MB, Kaelin WG. 2014b. Phosphorylation of ETS1 by src family kinases prevents its recognition by the COP1 tumor suppressor. *Cancer Cell* **26**:222–234. DOI: https://doi.org/10.1016/j.ccr.2014.06.026, PMID: 25117710

Matyskiela ME, Lu G, Ito T, Pagarigan B, Lu CC, Miller K, Fang W, Wang NY, Nguyen D, Houston J, Carmel G, Tran T, Riley M, Nosaka L, Lander GC, Gaidarova S, Xu S, Ruchelman AL, Handa H, Carmichael J, et al. 2016. A novel cereblon modulator recruits GSPT1 to the CRL4(CRBN) ubiquitin ligase. *Nature* **535**:252–257. DOI: https://doi.org/10.1038/nature18611, PMID: 27338790

Matyskiela ME, Zhang W, Man HW, Muller G, Khambatta G, Baculi F, Hickman M, LeBrun L, Pagarigan B, Carmel G, Lu CC, Lu G, Riley M, Satoh Y, Schafer P, Daniel TO, Carmichael J, Cathers BE, Chamberlain PP. 2018. A cereblon modulator (CC-220) with improved degradation of ikaros and aiolos. *Journal of Medicinal Chemistry* **61**:535–542. DOI: https://doi.org/10.1021/acs.jmedchem.6b01921, PMID: 28425720

Nakayama Y, Kosek J, Capone L, Hur EM, Schafer PH, Ringheim GE. 2017. Aiolos Overexpression in Systemic Lupus Erythematosus B Cell Subtypes and BAFF-Induced Memory B Cell Differentiation Are Reduced by CC-220 Modulation of Cereblon Activity. *The Journal of Immunology* **199**:2388–2407. DOI: https://doi.org/10.4049/jimmunol.1601725, PMID: 28848067

Neklesa TK, Winkler JD, Crews CM. 2017. Targeted protein degradation by PROTACs. *Pharmacology & Therapeutics* **174**:138–144. DOI: https://doi.org/10.1016/j.pharmthera.2017.02.027, PMID: 28223226

Pan ZQ, Kentsis A, Dias DC, Yamoah K, Wu K. 2004. Nedd8 on cullin: building an expressway to protein destruction. *Oncogene* **23**:1985–1997. DOI: https://doi.org/10.1038/sj.onc.1207414, PMID: 15021886

Perkins G, Drury LS, Diffley JF. 2001. Separate SCF(CDC4) recognition elements target Cdc6 for proteolysis in S phase and mitosis. *The EMBO Journal* **20**:4836–4845. DOI: https://doi.org/10.1093/emboj/20.17.4836, PMID: 11532947

Petroski MD, Deshaies RJ. 2005. Function and regulation of cullin-RING ubiquitin ligases. *Nature Reviews Molecular Cell Biology* **6**:9–20. DOI: https://doi.org/10.1038/nrm1547, PMID: 15688063

Petzold G, Fischer ES, Thomä NH. 2016. Structural basis of lenalidomide-induced CK1α degradation by the CRL4(CRBN) ubiquitin ligase. *Nature* **532**:127–130. DOI: https://doi.org/10.1038/nature16979, PMID: 26909574

Pickart CM. 2001. Mechanisms underlying ubiquitination. *Annual Review of Biochemistry* **70**:503–533. DOI: https://doi.org/10.1146/annurev.biochem.70.1.503, PMID: 11395416

Plon SE, Leppig KA, Do HN, Groudine M. 1993. Cloning of the human homolog of the CDC34 cell cycle gene by complementation in yeast. *PNAS* **90**:10484–10488. DOI: https://doi.org/10.1073/pnas.90.22.10484, PMID: 8248134

Qian X, Dimopoulos MA, Amatangelo M, Bjorklund C, Towfic F, Flynt E, Weisel KC, Ocio EM, Yu X, Peluso T, Sternas L, Zaki M, Moreau P, Thakurta A. 2018. Cereblon gene expression and correlation with clinical outcomes in patients with relapsed/refractory multiple myeloma treated with pomalidomide: an analysis of STRATUS. *Leukemia & Lymphoma*:1–9. DOI: https://doi.org/10.1080/10428194.2018.1485915, PMID: 30068263

Rodrigo-Brenni MC, Morgan DO. 2007. Sequential E2s drive polyubiquitin chain assembly on APC targets. *Cell* **130**:127–139. DOI: https://doi.org/10.1016/j.cell.2007.05.027, PMID: 17632060

Sakamoto KM, Kim KB, Kumagai A, Mercurio F, Crews CM, Deshaies RJ. 2001. Protacs: chimeric molecules that target proteins to the Skp1-Cullin-F box complex for ubiquitination and degradation. *PNAS* **98**:8554–8559. DOI: https://doi.org/10.1073/pnas.141230798, PMID: 11438690

Schafer PH, Ye Y, Wu L, Kosek J, Ringheim G, Yang Z, Liu L, Thomas M, Palmisano M, Chopra R. 2018. Cereblon modulator iberdomide induces degradation of the transcription factors ikaros and aiolos: immunomodulation in healthy volunteers and relevance to systemic lupus erythematosus. *Annals of the Rheumatic Diseases* **77**. DOI: https://doi.org/10.1136/annrheumdis-2017-212916, PMID: 29945920

Scott DC, Rhee DY, Duda DM, Kelsall IR, Olszewski JL, Paulo JA, de Jong A, Ovaa H, Alpi AF, Harper JW, Schulman BA. 2016. Two distinct types of E3 ligases work in unison to regulate substrate ubiquitylation. *Cell* **166**:1198–1214. DOI: https://doi.org/10.1016/j.cell.2016.07.027

Shibata E, Abbas T, Huang X, Wohlschlegel JA, Dutta A. 2011. Selective ubiquitylation of p21 and Cdt1 by UBCH8 and UBE2G ubiquitin-conjugating enzymes via the CRL4Cdt2 ubiquitin ligase complex. *Molecular and Cellular Biology* **31**:3136–3145. DOI: https://doi.org/10.1128/MCB.05496-11, PMID: 21628527

Skowyra D, Craig KL, Tyers M, Elledge SJ, Harper JW. 1997. F-box proteins are receptors that recruit phosphorylated substrates to the SCF ubiquitin-ligase complex. *Cell* **91**:209–219. DOI: https://doi.org/10.1016/S0092-8674(00)80403-1, PMID: 9346238

Soucy TA, Smith PG, Milhollen MA, Berger AJ, Gavin JM, Adhikari S, Brownell JE, Burke KE, Cardin DP, Critchley S, Cullis CA, Doucette A, Garnsey JJ, Gaulin JL, Gershman RE, Lublinsky AR, McDonald A, Mizutani H,

Narayanan U, Olhava EJ, et al. 2009. An inhibitor of NEDD8-activating enzyme as a new approach to treat cancer. *Nature* **458**:732–736. DOI: https://doi.org/10.1038/nature07884, PMID: 19360080

Winter GE, Buckley DL, Paulk J, Roberts JM, Souza A, Dhe-Paganon S, Bradner JE. 2015. DRUG DEVELOPMENT. phthalimide conjugation as a strategy for in vivo target protein degradation. *Science* **348**: 1376–1381. DOI: https://doi.org/10.1126/science.aab1433, PMID: 25999370

Wu K, Kovacev J, Pan ZQ. 2010. Priming and extending: a UbcH5/Cdc34 E2 handoff mechanism for polyubiquitination on a SCF substrate. *Molecular Cell* **37**:784–796. DOI: https://doi.org/10.1016/j.molcel.2010.02.025, PMID: 20347421

Zengerle M, Chan KH, Ciulli A. 2015. Selective small molecule induced degradation of the BET bromodomain protein BRD4. *ACS Chemical Biology* **10**:1770–1777. DOI: https://doi.org/10.1021/acschembio.5b00216, PMID: 26035625

Zhu YX, Braggio E, Shi CX, Bruins LA, Schmidt JE, Van Wier S, Chang XB, Bjorklund CC, Fonseca R, Bergsagel PL, Orlowski RZ, Stewart AK. 2011. Cereblon expression is required for the antimyeloma activity of lenalidomide and pomalidomide. *Blood* **118**:4771–4779. DOI: https://doi.org/10.1182/blood-2011-05-356063, PMID: 21860026